ANALYSIS OF ELECTRIC DOUBLE LAYER STRUCTURE FORMED DURING CORROSION OF STEEL PIPES CARRYING POTABLE WATER

BY

TANMAY SANJEEV GUPTE

Submitted in partial fulfillment of the requirements for the degree of
Masters of Science in Mechanical Engineering at
The University of Texas at Arlington
May, 2016

Arlington, Texas

Supervising Committee:
Dr. Bo Yang, Supervising Professor
Dr. Ratan Kumar
Dr. Dereje Agonafer

Acknowledgements

I am extremely grateful to my Supervising Professor Dr. Bo Yang, who gave me an opportunity to work under him in this project. It was his constant guidance and motivation that helped me complete the thesis. It was indeed a great learning experience working under him for my thesis. I am thankful to Dr. Ratan Kumar and Dr. Dereje Agonafer for serving on the committee panel to review my thesis. I am also thankful to my teammates Pranav Phadtare, Pratik Kale and Saurabh Deobhankar for helping me throughout this project. It would've been impossible to complete the thesis without your help and support.

I would like to thank my friends from Meadow Run 265, Garden Club 208 and my roommates from Cooper Chase 201 who emotionally supported me a lot unconditionally. I am extremely thankful to my parents and family members back in India who have always believed in me and encouraged me to pursue my dreams.

I would specially thank Debi and Flora for being so kind and helping me throughout the past two years.

Thank you all.

May 5, 2016

Abstract

ANALYSIS OF ELECTRIC DOUBLE LAYER STRUCTURE FORMED DURING CORROSION OF STEEL PIPES CARRYING POTABLE WATER

Tanmay Sanjeev Gupte, M.S

The University of Texas at Arlington, 2016

Supervising Professor: Dr. Bo Yang

Corrosion of steel pipes carrying drinking water is a universal issue. It affects human health as the corrosion sediments in these pipes can be toxic and unfit for consumption. Further, the amassing of the corrosion products can lead to operational difficulties. Drinking water consists of anions like carbonate, hydroxides and chloride ions which are responsible for the corrosion process. In such types of aqueous corrosion, there is an interfacial region formed between the corroding metal and the bulk of the aqueous environment. This interfacial region is called the Electrical Double Layer. In this article, we direct to study the effects on Double Layer Surface which takes place during the corrosion process. In order to develop an analytical model for simulation to obtain results in our system, we study and obtain certain chemical and physical properties of the chemical components in potable water such as Initial concentrations, Stokes radius, Ionic radii, relative permittivity etc. Results of the effects on the Double Layer Structure are obtained by varying certain parameters like electric

potential, metallic flux and temperature. From the results obtained, we notice that $CO3^{2-}$ anion is the single dominant factor causing corrosion in steel pipes. Concentration of $CO3^{2-}$ ion on the metal surface increases with voltage. At the same time, concentration of water on the surface reduces by increasing the voltage and eventually gets thrown off the metal surface.

Table of Contents

List of Illustrations

List of Tables

Chapter 1

Introduction

1.1 Corrosion: Basic Concept

Corrosion is fundamentally the result of interaction between the material and its environment. Damages caused by corrosion may result in loss of efficiencies of plants eventually leading to shutdowns and causing huge losses[1]. Corrosion in pipes carrying potable water is an extremely common phenomenon and a universal issue. It affects human health as the sediments of corrosion such as iron or copper are toxic and make it unfit for drinking.

1.2 Corrosion in Metal Pipes

Metal pipe corrosion is a continuous and variable process of ion release from the pipe into the water. Under certain environmental conditions, metal pipes can become corroded based on the properties of the pipe, the soil surrounding the pipe, the water properties [5]. When metal pipe corrosion occurs, it is a result of the

electrochemical electron exchange resulting from the differential galvanic properties between metals, the ionic influences of solutions, or the solution pH.

Fig 1.1: Corroded metal pipes [6]

1.3 Corrosion in Drinking Water Systems

For pipes carrying drinking water, use of lead pipes which was largely used earlier is now prohibited as its ions destroy brain cells. Similarly, in case of copper pipes which were widely used for domestic purposes, failures of certain types of copper corrosion were reported which included hot soft water pitting, sedimentation of copper etc [14].

Therefore, steel pipes are used in the conveyance of potable water. Galvanization offers as a means for corrosion resistance for steel. However, due to cost considerations the applications are restricted to domestic use only. Irrespective of the material, pipes would not corrode if the water were not aggressive. [14]

Drinking water also known as potable water contains cations such as H^+,Ca^{2+}, Na^+, Mg^{2+}, K^+ etc. and anions like OH^-, $CO3^{2-}$, $HCO3^-$, Cl^-. Desalinated potable water is considered to be very aggressive. Corrosion is usually induced by presence of anions however, there are other factors as well that cause corrosion.

Key water quality parameters that are expected to influence corrosion include pH, alkalinity, and buffer intensity.

Role of pH: Weight loss is generally found to increase with increasing pH in the range 7 to 9

Alkalinity: Increasing alkalinity generally leads to lower weight loss and corrosion rate.

Buffer Intensity: Higher buffer intensity is often associated with increased alkalinity, although the two parameters are not exactly equivalent. However, their effect on iron corrosion seems to be similar. Several studies found the maximum weight loss for cast iron samples occurred at the minimum buffer intensity (pH 8.4)

presumably because higher buffer intensity attenuates pH changes due to corrosion reactions at anodic and cathodic areas.

1.4 Corrosion Mechanism

For corrosion to occur there must be an anode and a cathode and an electric potential between. Both must be immersed in an electrolytic fluid which must be electrically conductive [19]. Thus, corrosion is basically an electrical circuit where electrons flow from anode to cathode. When electrons flow from anode, the anode oxidizes to form metallic ions [19]. These ions then flow towards the cathode through the electrolyte.

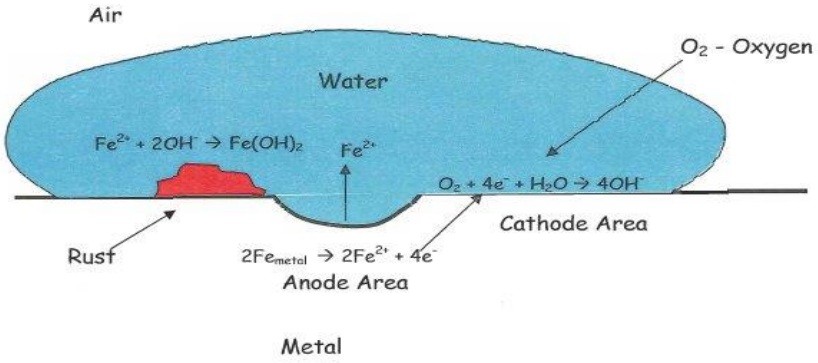

Figure 1.2: Corrosion Mechanism[19]

1.5 Corrosion and Chemical Reactions in our sytem(Steel Pipes carrying drinking water)

In our system, when iron corrodes in water, metal ions leave the lattice and enter the electrolyte as ferrous ions.

In absence of other oxidants, electrons released in oxidation of iron are consumed in reduction of oxygen.

Anodic Reaction: $Fe = Fe^{2+} + 2e^{-}$

Cathodic Reaction: $O_2 + 4H^{+} + 2e^{-} = 4(OH)^{-}$

Ferrous ions and hydroxide ions react to form highly reducible ferrous hydroxide

$2Fe^{2+} + 4\ OH^{-} = 2Fe(OH)$.

Ferrous hydroxide is oxidized to ferric hydroxide by O2:

4 Fe (OH)2 + O2 +2H2O = 4Fe(OH)3.

In the electrolytic solution, drinking water contains Calcium and Bicarbonate ions. Bicarbonate ion is slowly neutralized to Carbonate ion

HCO3 (-) + OH (-) = CO3 (2-) + H2O

Resulting CO3 (2-) would precipitate CaCO3 on the metal surface:

$Ca(2+) + CO3(2-) = CaCO3$

Our main focus is to study about the effects on the Double Layer. Thus it is very important to know about the basics of Electrical Double Layer. We study about EDL in detail in this and the next section.

1.6 Electric Double Layer: A Bird's eye view

In aqueous corrosion, an interfacial layer is formed between a corroding metal and the bulk of the aqueous environment. This interfacial layer is called the Double Layer [7]. In an electrical circuit used to measure current flowing at a particular working electrode, the Double Layer can be viewed as a capacitor. In the double layer, the water molecules of the solution align themselves with the electric field generated by applying a potential to the metal [9]. Double Layer structure depends on several parameters such as material of the electrode, type of solvent, extent of adsorption of specific ions and molecules and temperature [7].

1.7 Double Layer Models

The concept of the existence of the double layer at the surface of a metal being in contact with an electrolyte was put forward by Helmholtz in 1879. In this model he assumed that no electron transfer reactions occur at the electrode and the solution is composed only of electrolyte. Two layers of opposite polarity are formed at the interface between electrode and electrolyte [8]. The interactions between the ions in solution and the electrode surface were assumed to be electrostatic in nature and resulted from the fact that the electrode holds a charge density which arises from either an excess or deficiency of electrons at the electrode surface. Helmholtz Double Layer comprises of two layers: Inner Helmholtz Plane (IHP) and Outer Helmholtz Layer (OHP) [8]. Water molecules are attracted towards the metal electrode and form the first adsorbed layer on the metal surface. This is the IHP. The cations which are hydrated are attracted towards the metal surface. However, their approach towards the metal surface is limited because of the presence of water molecules on the metal surface. The OHP comprises of the locus of electrical centers of these positive charges.

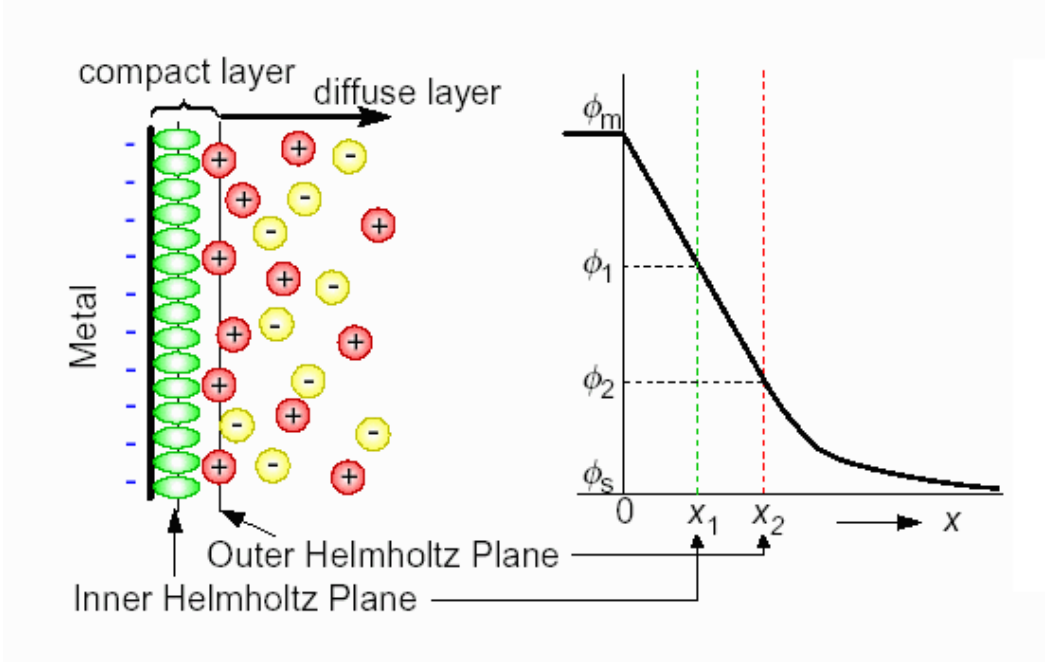

Fig 1.3: Electric Double Layer Structure [8]

The next model, of Gouy and Chapman, involves a diffuse double layer in which contains the excess cations or anions. They extend to some distance from the solid surface. Electric potential decreases exponentially way from the surface.

In further developments, Stern (1924) suggested that the electrified solid-liquid interface includes both the rigid Helmholtz layer and the diffuse one of Gouy and Chapman. His theory states that ions do have finite size, so cannot approach the surface closer than a few nm.

1.8 Objective

The main objective of our research is to analyze the effects on the Electric Double Layer structure formed on the corroded steel surface of the pipes carrying drinking water by changing parameters like electric potential, temperature.

Chapter 2

Mathematical Approach to the Electrical Double Layer Theory

The EDL theory can be described using Fick's law of mass transport, Gauss's law of electrostatics and Newton's law of force balance. During corrosion process, ions need to move around or be transported in the solution. Diffusion is the process where these species move under the action of concentration gradient. Through numerical examples, reasonable double layer structures can be predicted [12].

THEORY OF AN ELECTRIC DOUBLE LAYER

2.1 Chemical Potential

An electrolyte consists of mobile ions and polarizable solvent molecules. The chemical potential per particle is given by

$$\mu_i = k_B T \ln(n_i) + z_i e\phi - \int_0^{\boldsymbol{\tau}_i} \nabla\phi \cdot d\boldsymbol{\tau}_i + \gamma_i p, \qquad (1)$$

where k_B is the Boltzmann constant, T is the temperature, ϕ is the electrostatic potential, p is the hydrostatic pressure, e is the unit charge, and n_i, z_i, γ_i and $\boldsymbol{\tau}_i$ are the number concentration, the valance number, the chemical expansion volume, and the induced dipole moment of the i^{th} component, respectively. The index i covers all independent constituents including ions and solvent molecules. The four terms represent the effects of entropy, charge, dipole moment and mechanical pressure, respectively [12].

Langevin equation is given by

$$\boldsymbol{\tau}_i = -\epsilon_0 \chi_i \nabla\phi, \text{ with } \chi_i \equiv \frac{3}{\bar{\tau}_{0i} E}\left(\coth(\bar{\tau}_{0i} E) - \frac{1}{\bar{\tau}_{0i} E}\right)\chi_{0i} \text{ and } \bar{\tau}_{0i} = \frac{\tau_{0i}}{k_B T}, \qquad (2)$$

It is devised to describe the polarization of solvent molecules and ions carrying permanent dipole moment. where ϵ_0 is the permittivity of vacuum, χ_{0i} and τ_{0i} are the linear polarization susceptibility per particle and the (permanent) dipole moment per particle of the i^{th} component, and $E = |\nabla\phi|$. The Langevin equation is strictly only applicable to orientation polarization of permanent dipoles. We extend it here to describe all possible polarization mechanisms including electronic as well as orientation type so that a concise form as above can be presented relating the total polarization strength to measurable linear susceptibility χ_{0i}. Substituting Eq. (2) in the third term on the right-hand side of Eq. (1) and integrating, we get

$$-\int_0^{\boldsymbol{\tau}_i} \nabla\phi \cdot d\boldsymbol{\tau}_i = k_B T \left(\ln\left(\frac{\sinh \bar{\tau}_{0i} E}{\bar{\tau}_{0i} E} \right) - \bar{\tau}_{0i} E \coth(\bar{\tau}_{0i} E) + 1 \right). \quad (3)$$

In Eq. (1), the first two terms of thermal and electrostatic charge forces are considered in the classical PNP formulation, widely applied in decades. Dipolar-Poission-Boltzman….. Quiroga et al. attempted to include the term of electrostatic polarization effect [13]. However, their expression seems only appropriate for constant (rather than induced) dipoles always in alignment with electrical field $-\nabla\phi$. Meanwhile, they applied the Langevin equation for the dipole moment in controversy. Nevertheless, the importance of the idea to include this term of polarization effect in the chemical potential cannot be overlooked. Only if it was included, active transport of dipolar molecules towards a charged surface could be captured, which can be important in many applications, such as corrosion, where concentrations of not only ions but also neutral molecules (e.g., water) are required to be accurately known [12].

2.2 Dynamic Transport and Other Field Governing Equations

According to Fick's first law, the flux of the i^{th} species may be expressed as $\boldsymbol{j}_i = -M_i n_i \nabla\mu_i$, in which M_i is the mobility of the i^{th} species that can be a complex function of concentrations of all components. By

substituting Eq. (1) in the flux equation and effecting Einstein's relation $D_i = M_i k_B T$, the flux of the i^{th} species is obtained as

$$\boldsymbol{j}_i = -D_i \nabla n_i + n_i \left[M_i \left(-z_i e \nabla \phi + \frac{\epsilon_0 \zeta_i}{2} \nabla (\nabla \phi \cdot \nabla \phi) - \gamma_i \nabla p \right) + \boldsymbol{u} \right], \tag{4}$$

where $\boldsymbol{u}$ is the velocity, and electric field-dependent constant ζ_i is given by

$$\zeta_i = 3 \left(\frac{1}{(\bar{\tau}_{0i} E)^2} - \coth^2(\bar{\tau}_{0i} E) + 1 \right) \chi_{0i}. \tag{5}$$

The above constant $\zeta_i \cong \chi_{0i}$ if $\bar{\tau}_{0i} E \ll 1$. According to the law of mass conservation, the equation of dynamic transport is given by

$$\frac{\partial n_i}{\partial t} = -\nabla \cdot \boldsymbol{j}_i + R_i, \tag{6}$$

where t is the time, and R_i is the production rate of the i^{th} component from chemical reaction.

In order to complete the formulation, two additional field governing equations are required for the electrostatic potential and the pressure, respectively. For the electrostatic potential field, the Gauss' law/Poisson's equation is applied:

$$\nabla \cdot \epsilon_0 (1 + \textstyle\sum_i \chi_i n_i) \nabla \phi + \sum_i z_i e n_i = 0, \tag{7}$$

where the second term is the total charge density due to the separation of counterions and coions, and the electric field-dependent susceptibility χ_i is given in Eq. (2). It is assumed that the polarization effect is additive from all constituents [12].

By assuming that the electrolyte is a compressible Newtonian fluid, the equilibrium equation according to Newton's law is given by

$$-\nabla p + \nabla \cdot \eta \left(\nabla \boldsymbol{u} + \nabla^T \boldsymbol{u} - \frac{2}{3}\mathbf{I}\nabla \cdot \boldsymbol{u}\right) - \sum_i z_i e n_i \nabla\phi + \frac{1}{2}\epsilon_0 \sum_i \zeta_i n_i \nabla(\nabla\phi \cdot \nabla\phi) = 0, \quad (8)$$

where the hydrostatic pressure p is due to "elastic" deformation, given by an equation of state, the second term is due to viscous flow, the third term is the electrostatic charge force density, and the fourth term is the electrostatic polarization force density due to induced dipoles. It is well known that the electrostatic charge force density can be expressed as the divergence of Maxwell's stress. In contrast, the above electrostatic polarization force density of Langevin dipoles is derived from the Korteweg-Helmholz method, and reported here for the first time. It is consistent to the thermodynamic force for mass transport in Eq. (4), which is no surprise since the Korteweg-Helmholz method is devised following the same principle on basis of the chemical potential. It might be worth mentioning that several different expressions of Korteweg-

Helmholz force density can be found in various papers and textbooks. They are typically results of further derivation under certain conditions. The present electrical force density is derived directly from Eq. (15) in Sec. 3.7 in reference[1]. It might also be worth noting that the above third term of polarization force density reduces to the Kelvin force density $\left(\equiv \frac{1}{2}\epsilon_0 \sum_i \chi_i n_i \nabla(\nabla\phi \cdot \nabla\phi)\right)$ when $\bar{\tau}_{0i}E \ll 1$. In other words, the Kelvin force density, defined by simply multiplying the induced dipole moment with electric field gradient, is inapplicable in the nonlinear case of Langevin's dipoles. The microscopic forces that individual induced dipoles (in average) experience do not always add up linearly as the macroscopic electrical force [14].

Lastly, rate-independent hydrostatic pressure p is expressed in an EOS as $p = p(N, V, T)$, where $N(\equiv \sum n_i)$ is the total number of particles per unit volume, and $V(\equiv \sum \nu_i = \sum n_i \gamma_i)$ is the packing density. The well-known Carnahan-Starling EOS for repulsion[2] plus van der Waals attraction term[3] is adopted, which is given by

$$\frac{p}{Nk_BT} = \frac{1+V+V^2-V^3}{(1-V)^3} - \frac{a}{k_BT}, \tag{9}$$

with $a = \sum n_i a_{ij} n_j$, where a_{ij} describes the attractive interaction effect between species i and j. Note that we generalize it for multicomponent mixtures, with $a_{ij} = \sqrt{a_{ii} a_{jj}}$, similar to how the literature has treated the Lennard-Jones potential for mixtures[4]. Constant a_{ii} for a single component can be found from the pressure and temperature at the critical liquid-vapor point.

2.3 Finite Volume Method for One-dimensional Planar Problems

A finite volume method is adopted to numerically solve the above set of governing equations (Eqs. (6)-(9)) along with appropriate initial-boundary conditions for fields n_i, ϕ, $\boldsymbol{u}$ and p in one-dimensional planar problems of an EDL. By the virtue of a finite volume method, the first step is to present the problem of a divergence equation governing a field over a domain with surface integrals of flux according to the divergence theorem. This is applied to each one of the cells (i.e., finite volumes) used to discretize the whole domain. The flux at cell boundaries is then approximately evaluated from nodal values of a field defined within the cells. When the flux, though approximate, is applied identically to adjacent cells sharing the

surface where it is defined, the law of conservation of the field quantity is always satisfied. Since the present multi-physics problem is highly nonlinear, an iterative scheme is indispensable [12].

Let us discretize a one-dimensional finite domain into M cells, numbered in order from 1 to M. Each cell is assigned with a node at the middle point. Potential ϕ, concentration n_i and velocity $\boldsymbol{u}$ are the basic quantities, and are defined on the nodes. There are M nodal degrees of freedom for either one of ϕ, n_i or $\boldsymbol{u}$. Thus, one needs to gather M algebraic equations to solve for each one of them. This is attained by applying Eqs. (6)-(8) to each cell. Based on the nodal values, the fields of ϕ, n_i and $\boldsymbol{u}$ near a knot m are approximated as

$$\phi(x;x^m) = \sum_q N_q^m(x)\phi_q, \tag{10a}$$

$$n_i(x;x^m) = \sum_q N_q^m(x)n_{iq}, \tag{10b}$$

$$\boldsymbol{u}(x;x^m) = \sum_q N_q^m(x)\boldsymbol{u}_q, \tag{10c}$$

where superscript m indicates the m^{th} knot, subscript q indicates the q^{th} node selected to approximate the field around knot m, and $N_q^m(x)\left(=\prod_{p\neq q}\left(\frac{x-x_p}{x_q-x_p}\right)\right)$ is the Lagrange interpolation function in terms of selected nodal coordinates around knot m. In later numerical examples, two nodes from the left side and two

nodes from the right side, if available, are chosen to approximate a field about a knot. For knots near the ends (i.e., domain boundary), lower-rank interpolation is used, since there may be less than two nodes available on the end side. Derivatives and integrals of these fields around a knot can be conveniently obtained from Eq. (10). For the sake of brevity, their explicit expressions are not presented here.

By applying the divergence theorem, the governing equation of electrostatics (Eq. (7)) over the m^{th} cell between knots m-1 and m is turned into

$$\epsilon^{m,l}\left(\phi_{,x}\right)^{m,l+1} - \epsilon^{m-1,l}\left(\phi_{,x}\right)^{m-1,l+1} + \sum_i z_i e n_{im}^{l} (\Delta x)_m = 0, \qquad (11)$$

where $\epsilon^{m,l} \equiv \epsilon_0\left(1 + \sum_i \chi_i^{m,l} n_i^{m,l}\right)$, valid for $\epsilon^{m-1,l}$ as well, $(\Delta x)_m$ is the cell size, superscript l after comma indicates the l^{th} iterative step, and subscript comma indicates partial differentiation with respect to the indices that follow. Again, superscript m (or m-1) in the first two terms indicates that ϵ and $\phi_{,x}$ are evaluated at knot m (or m-1) based on nearby nodal values by Eq. (10) and its derivatives. For example, $\left(\phi_{,x}\right)^{m,l+1} = \sum_q N_{q,x}^{m}(x = x^m)\phi_q^{l+1}$. By assuming that all quantities at the l^{th} iterative step are known, Eq. (11) offers an algebraic equation of unknown nodal values of potential at the $(l+1)^{\text{th}}$ iterative step.

Similarly, the governing equations of mass transport (Eqs. (4) and (6)) within the m^{th} cell between knots m-1 and m are turned into

$$\frac{(\Delta x)_m}{\Delta t}\left(n_{im}^{\prime,l+1} - n_{im}^{0}\right) + \left(j_i^m - j_i^{m-1}\right) - (\Delta x)_m R_{im} = 0, \tag{12a}$$

$$j_i^* = -D_i^{*,l}\left(n_{i,x}\right)^{*,l+1} + (A^{*,l} + u^{*,l})n_i^{*,l+1}, \text{ with } *= m, m-1, \tag{12b}$$

$$A \equiv M_i\left(-z_i e\phi_{,x} + \epsilon_0 \zeta_i \phi_{,x}\phi_{,xx} - \gamma_i p_{,x}\right), \tag{12c}$$

where n_{im}^0 is the nodal concentration at the previous time step, and Δt is the time step. Though more complicated, Eq. (12) works the same as Eq. (11) to offer an algebraic equation of unknown nodal values of n_i at the (l+1)$^{\text{th}}$ iterative step given all quantities at the previous iterative step. Above p is computed from Eq. (9). The time rate-of-change term in Eq. (6) is treated above as a source term with time-marching step Δt. Meanwhile, all other terms/quantities involved in Eq. (4) of j_i are evaluated at the current time step; thus, an implicit finite difference scheme is used to treat the temporal dynamics of the problem.

Furthermore, the equilibrium equation of force balance (Eq. (8)) over the m^{th} cell between knots m-1 and m are turned into

$$-(p^{m,l} - p^{m-1,l}) + \frac{4}{3}\left(\eta^{m,l}\left(u_{,x}\right)^{m,l+1} - \eta^{m-1,l}\left(u_{,x}\right)^{m-1,l+1}\right) + (\Delta x)_m f_m = 0, \quad (13a)$$

$$f = -\sum_i z_i e n_i \nabla\phi + \frac{1}{2}\epsilon_0 \sum_i \zeta_i n_i \nabla(\nabla\phi \cdot \nabla\phi). \quad (13b)$$

This set of algebraic equations is solved for velocity field u at each iteration step.

Equations (11)-(13) are only applicable to interior cells. For boundary cells, the quantities evaluated at the knot at the boundary end should be replaced by a prescribed boundary condition. If a flux boundary condition is prescribed, the replacement is straightforward. If a potential/concentration boundary condition is prescribed, it is converted into a flux boundary condition with a penalty coefficient. For instance, for diffusion at the far end (i.e., knot M), it is written: $j_i^M = k^M(n_i^M - \bar{n}_i^M)$, where k^M is the penalty coefficient, a numerical parameter, $\bar{n}_i^M$ is the prescribed value of concentration, and n_i^M is the concentration at knot M and expressed in terms of two nodal values next to the end by Eq. (10). If k^M is set sufficiently large, $n_i^M = \bar{n}_i^M$ is approximately obtained, with controlled, negligible numerical error.

The solution procedure is briefly described as follows. Given appropriate initial and boundary conditions, the problem is solved incrementally in time and iteratively over each time step. Marching in time poses little

issue in this case of a parabolic problem in nature. For each iterative step l+1, a system of algebraic equations with nodal potential ϕ_m^{l+1} as variables and all coefficients and other quantities evaluated from previous iterative step l is assembled from Eq. (11). The stiffness matrix is inverted to solve for nodal potentials at the $(l+1)^{\text{th}}$ iterative step. Then, nodal concentrations of the first chemical component at the $(l+1)^{\text{th}}$ iterative step is solved by inverting the stiffness matrix assembled from Eq. (12) with i =1. This is repeated until nodal concentrations of all chemical components are updated. Finally, Eq. (13) is solved to update velocity u. However, since the present problem is highly nonlinear, especially when concentrations reach their saturation values, this scheme with no relaxation may become unstable. Instead, the following over-relaxation scheme is used; for instance, for potential, $\phi_m^{l+1} = \phi_m^l + \alpha\Delta\phi_m$, where $\Delta\phi_m$ is the difference of above obtained new value of ϕ_m from ϕ_m^l, and α is the relaxation factor. Typically a larger α leads to faster convergence, but greater chance of numerical instability. Trials are needed to identify reasonable value of α.

Chapter 3

Numerical Analysis and Results

3.1 Simulation Model and Problem Formulation

The objective of this section is to describe the work done in developing the analytical model to study the behavior of corrosion and effects on the Double Layer in our system. This firstly involves studying our system (potable water and steel pipes) and obtaining the physical and chemical parameters of the chemical components in the system. The chemical parameters basically include concentrations of the components present in the electrolyte. The physical parameters include Stokes radius, Physical Radius, Relative Permittivity etc.

Problem Formulation

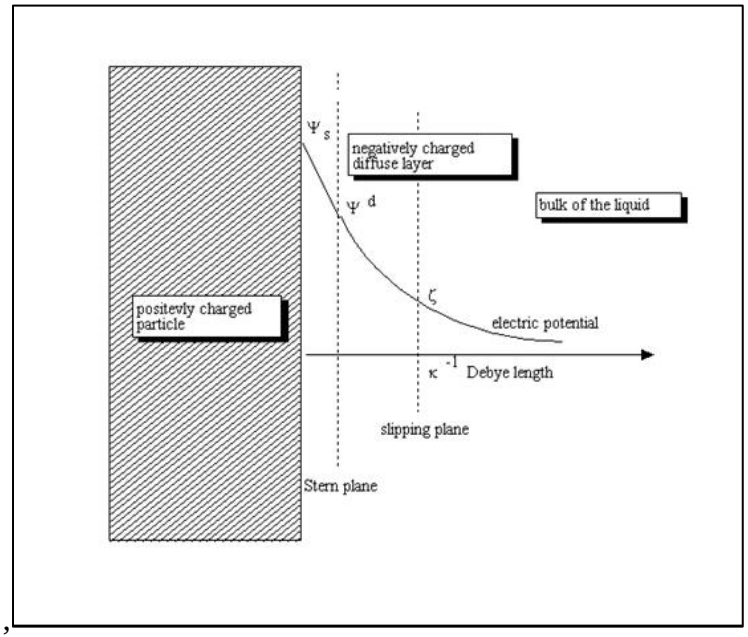

Figure 3.**Error! No text of specified style in document.**1:Problem Formulation of EDL Structure

EDL is formed basically when an electrode is immersed in an electrolyte. In our case, Steel pipe is the electrode and drinking water is the electrolyte. Electro neutrality has been maintained in the electrolyte i.e. charges are balanced. The problem reduces to 1-D planar problem.

We apply a fixed electric potential on the metal surface which decreases to zero at infinite distance. Other boundary conditions include temperature of the system, metallic flux etc. Initial concentrations of the components in the electrolyte are fixed as shown in section 3.1.1.

3.1.1 Chemical Parameters

The chemical components of drinking water are mainly $Ca^{2+,}$ Mg^{2+}, Na^{+}, H^{+}, OH^{-}, CO3(2-) , Cl(-) etc.. However, corrosion process occurs mainly due to presence of the anions. Our first step includes determining the initial chemical concentrations of these chemical components. We obtain the following results for the initial concentration of the chemical components in drinking water.

COMPONENT	CONCENTRATION(particle/nm3)
H2O	32.7
Ca^{2+}	2.6e-3
CO3(2-)	2.01e-3
H(+)	6.02e-7
OH(-)	6.02e-7
Cl(-)	1.7e-4

Table 1: Initial Concentration of Components in Water [15]

3.1.2 Physical Parameters

The next review is about the physical parameters of components in the electrolyte as well as the electrode. This also includes the products formed before and during the corrosion process such as salts formed in the electrolyte like Calcium Carbonate (CaCO3) and Magnesium Chloride(MgCl2) and also the products formed on the metal surface viz. Fe(OH)2, Fe(OH)3 and FeCl2.

Physical parameters include Relative permittivity, Stokes radius, Ionic radii, Viscosity and Vander Waal's constant. We determine these parameters at a temperature range of 273-323 K.

COMPONENT	RELATIVE PERMITTIVITY(V/nm)
H2O	79
Ca(2+)	3
CO3(2-)	2
H(+)	0
OH(-)	64.4
Cl(-)	10
O2	6.89
Mg(2+)	7.6
Fe(2+)	16
Fe(3+)	15.8
FeCl2	14.2
CaCO3	9.1
MgCl2	5.6

Table 2: Relative Permittivity of Components [18]

Stokes radius can be determined by the following formula,

$$R_H = a = \frac{k_B T}{6\pi\eta D}$$

kB is the Boltzman factor

T is the temperature in Kelvin = 300 K

η is the viscosity of the fluid

D is the Diffusion constant of the component at the given temperature

COMPONENT	STOKES RADIUS(nm)	IONIC RADIUS(nm)
H2O	0.09687	0.1552
Ca(2+)	0.0344	0.099
CO3(2-)	0.03086	0.178
H(+)	0.0244	0.1552
OH(-)	0.0431	0.137
Cl(-)	0.1082	0.181
O2	0.109	0.135
Mg(2+)	0.311	0.072

COMPONENT	STOKES RADIUS(nm)	IONIC RADIUS(nm)
Fe(2+)	0.3851	0.06
Fe(3+)	0.3861	0.07
FeCl2	0.4613	0.2246
CaCO3	0.0344	0.0348
MgCl2	0.311	0.1847

Table 3: Stokes Radius and Ionic Radius of Components[16][17]

3.1.3 Truncation Length

We need to fix the truncation length also known as the simulation domain. This length is basically the distance from the electrode i.e. width of the double layer structure we consider for our analysis. This distance can be determined by calculating the Debye Screening Length.

Debye Length is basically the distance till which the electrostatic effect persists. It can be calculated by

$$\kappa^{-1} = \sqrt{\frac{\varepsilon_r \varepsilon_0 k_B T}{2 N_A e^2 I}}$$

k^{-1} = Debye Length

T = Temperature in Kelvin

N_A = Avogadro's Number

e = Elementary Charge

I = Ionic Strength in (mole/m^3)

ε_r = Dielectric Constant

ε_0 = Permittivity of Free space

k_b = Boltzmann Constant

By calculating, Debye Length comes out to 1.5 nanometers. However, we consider other distances also as sometimes the Debye Length calculated can be smaller than ionic radii of certain components. In some cases, it is too large that the electric potential drops to zero at a smaller distance. Hence, we consider truncation lengths from 0.5 nm to foresee all parameters. Plots for Concentration of Components vs Distance from the Electrodes for different truncation lengths are as follows.

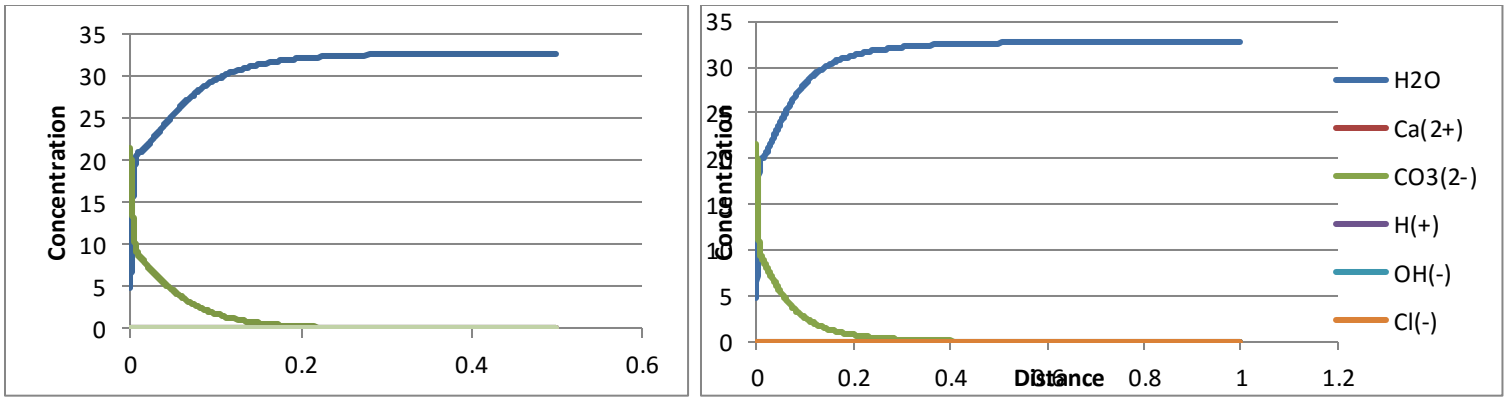

Figure 3.2: Concentration of Components vs Distance from Electrode at 0.5nm and 1nm

For truncation length of 0.5 and 1 nanometer, we do not get stable results and the voltage does not converge over the given distance. Hence, we cannot consider 0.5nm and 1nm as our simulation domain length

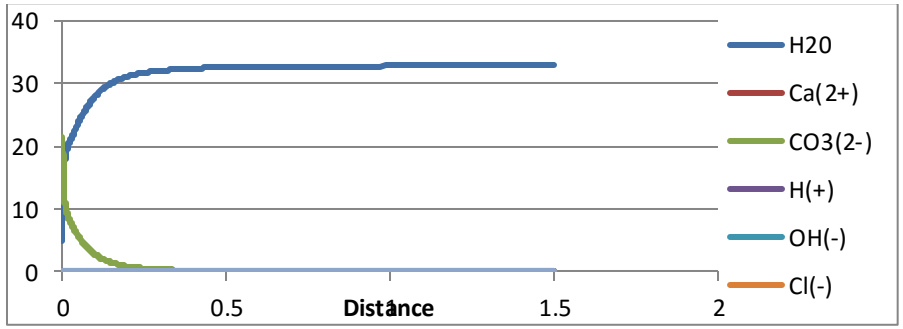

Figure 3.3:Concentration vs Distance from Electrode for 1.5nm

For 1.5 nm, results yielded are much stable and electric potential converges to zero over the given distance. Hence, we consider 1.5nm as our simulation domain.

3.2 Simulation and Results

After developing the analytical model based on the Double Layer theory, we run the simulation by adjusting and varying certain parameters such as Electric Potential, temperature and pH value. Results obtained from the simulation about the effects of these parameters on the EDL can be interpreted by graphical methodology as shown below.

3.2.1 At 300K Temperature and Electric Potential varying from 0.2V (Without considering metallic flux)

Initially, we only analyze the EDL by varying voltage from 0 to 2V in certain steps keeping temperature and pH value constant (300 K and pH=7).

We maintain the concentrations of the components mentioned above as our boundary conditions keeping the spring coefficient at 1000. For this case, it must be noted that we are not considering the flux applied to presence of the metallic ions.

3.2.1.1 Concentration of Components vs Distance from Electrode

At 0.2 V

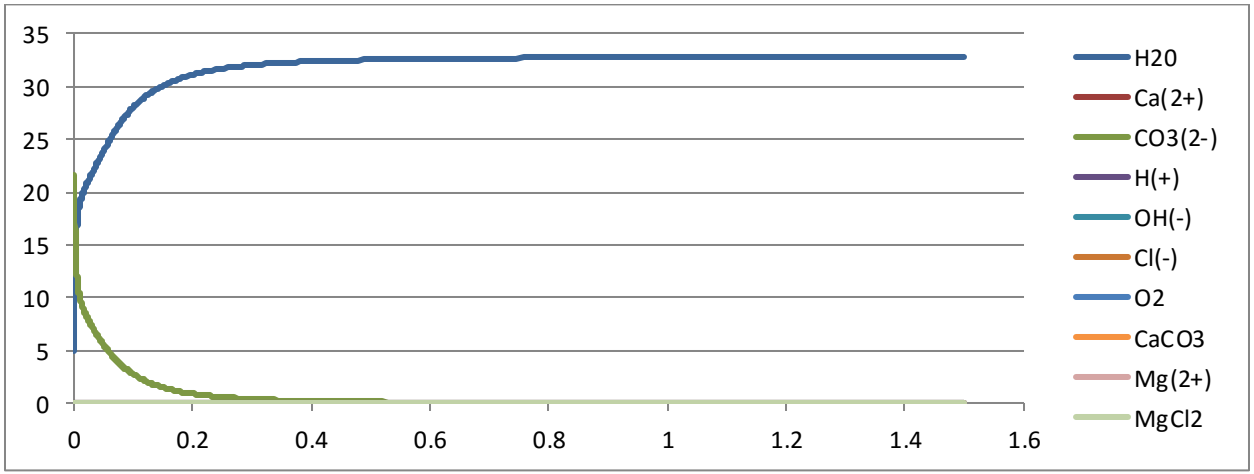

Fig 3.4: Concentration of components vs Distance from the Electrode at 0.2 V (Major Components)

At this voltage, CO_3^{2-} is most dominant ion on the metal surface, 21.57 part/nm^3. Concentration of H_2O is still high on the metal surface. Other anion concentration on the surface is comparatively lower. Concentration of $(OH)^-$ ion is 0.001 part/nm^3 and Cl^- is 0.006 part/nm^3.

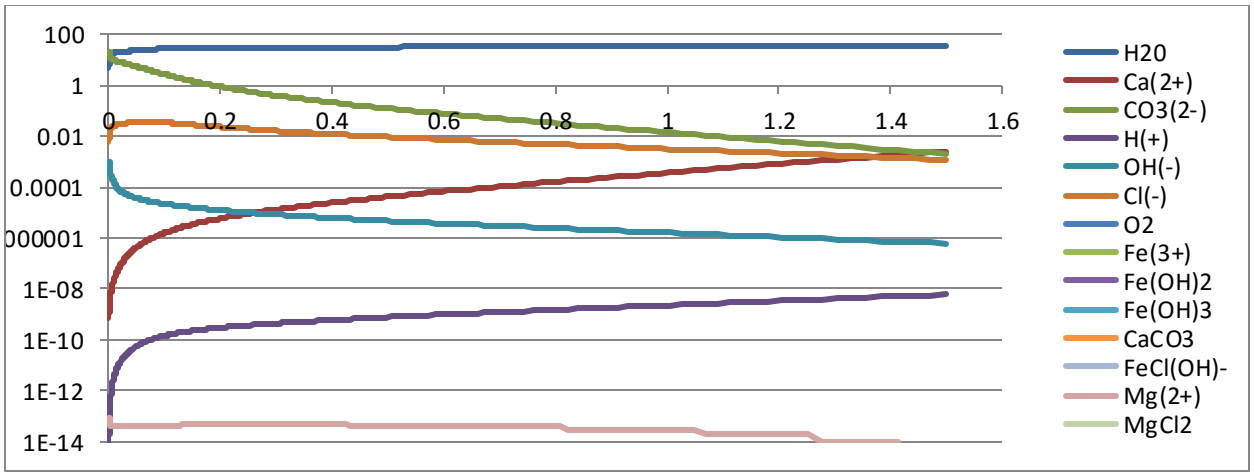

Fig 3.5: Concentration of components vs Distance from the Electrode at 0.2 V (Other Components present in smaller quantities)

At 0.5 V

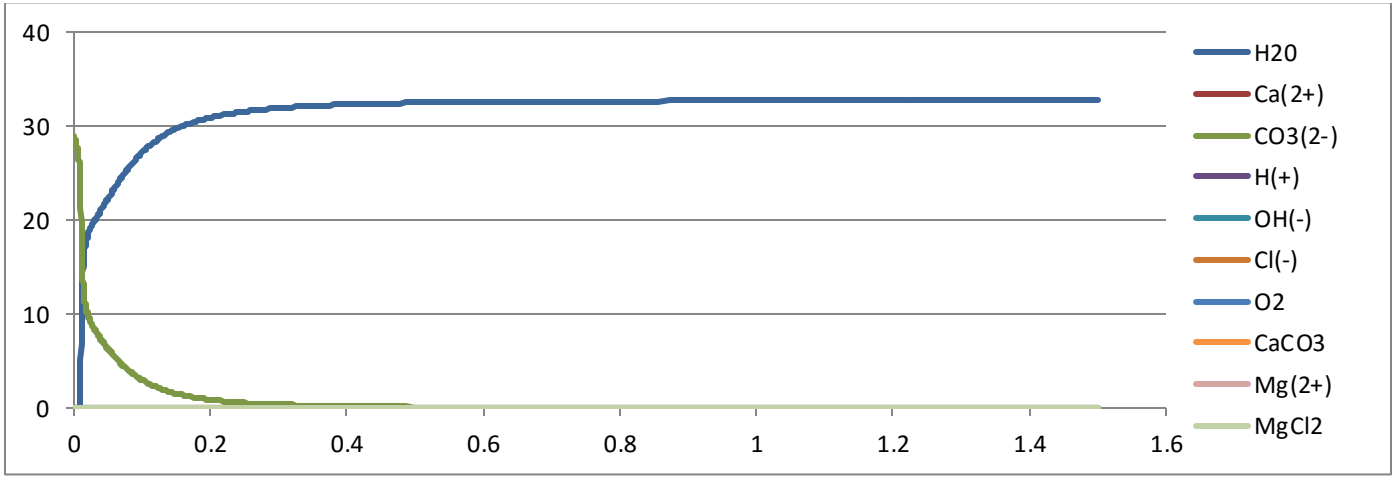

Fig 3.6: Concentration of components vs Distance from the Electrode at 0.5 V (Major Components)

CO_3^{2-} concentration is still dominant on the metal surface with its concentration increasing to 29 part/nm^3. Water concentration decreases on the metal surface. As shown below, the concentration of other anions.$(OH)^-$ concentration increases to 0.003 part/nm3 but Cl^- decreases.

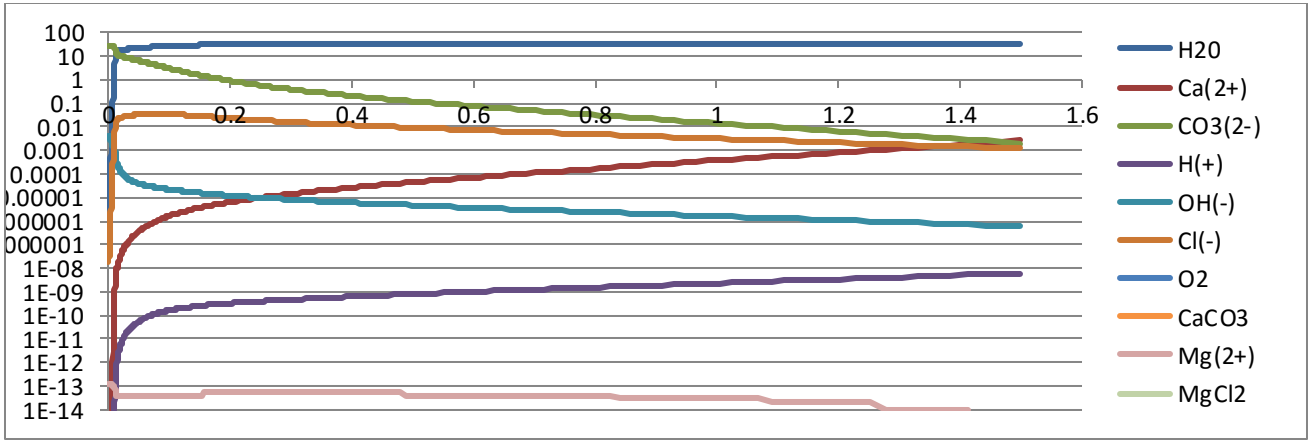

Fig 3.7: Concentration of components vs Distance from the Electrode at 0.5 V (Other Components present in smaller quantities)

At 0.8V

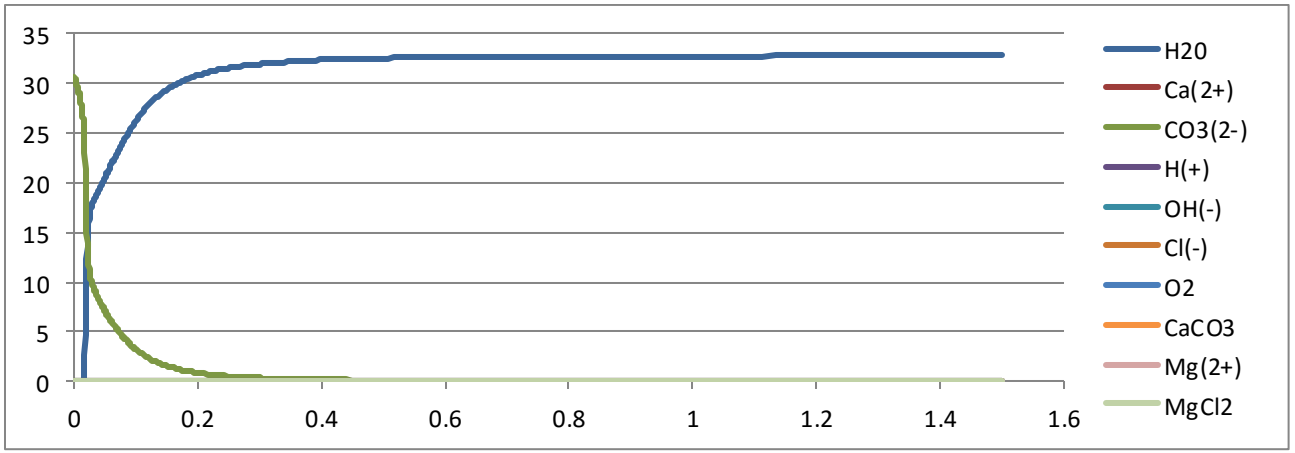

Fig 3.8: Concentration of components vs Distance from the Electrode at 0.8 V (Major Components)

At this voltage, carbonate ion still dominates on the surface of the metal with a concentration of 30.08 part/nm^3. As shown below, $(OH)^-$ ion concentration increases to 0.01 part/nm^3 and Cl^- further reduces.

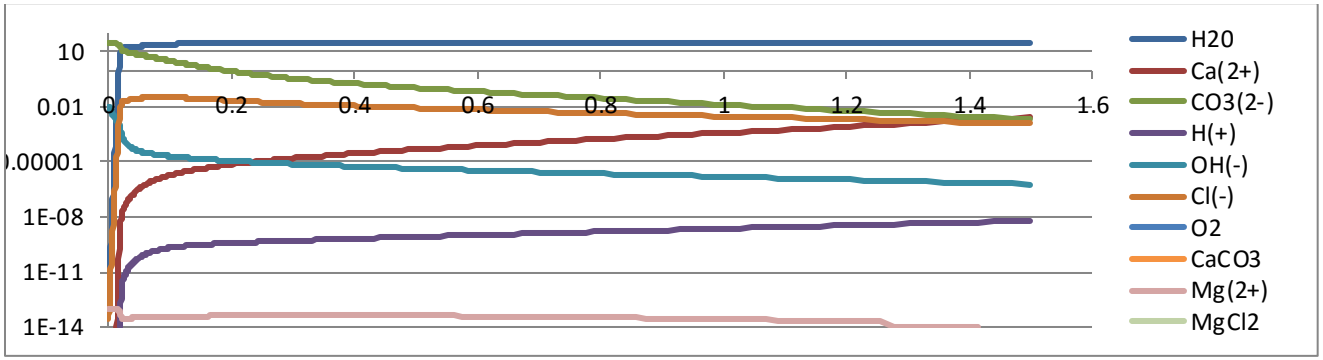

Fig 3.9: Concentration of components vs Distance from the Electrode at 0.8 V (Other Components present in smaller quantities)

At 1V

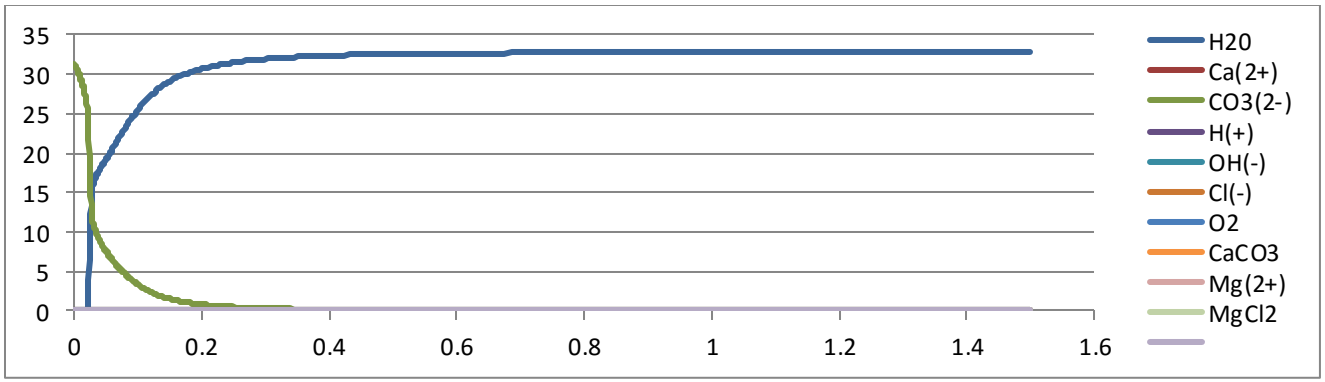

Fig 3.10: Concentration of components vs Distance from the Electrode at 1 V (Major Components)

At 1V, CO_3^{2-} ion concentration still dominant on the metal surface is 31.4 part/nm^3. As shown below the graph showing detailed concentration of other ions, it can be OH^- ion concentration on the metal surface increases to 0.2 part/nm^3. Water concentration on the surface is further reduced.

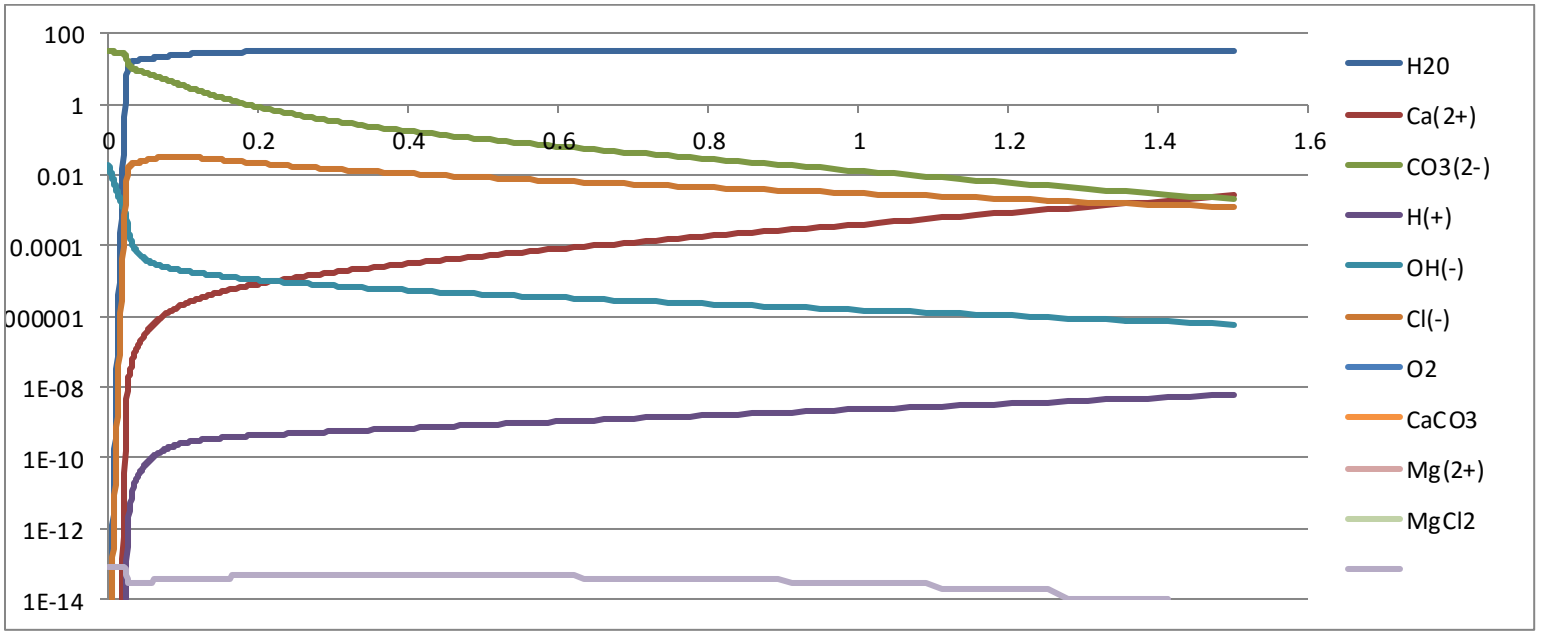

Fig 3.11: Concentration of components vs Distance from the Electrode at 1 V (Other Components present in smaller quantities)

At 1.5V

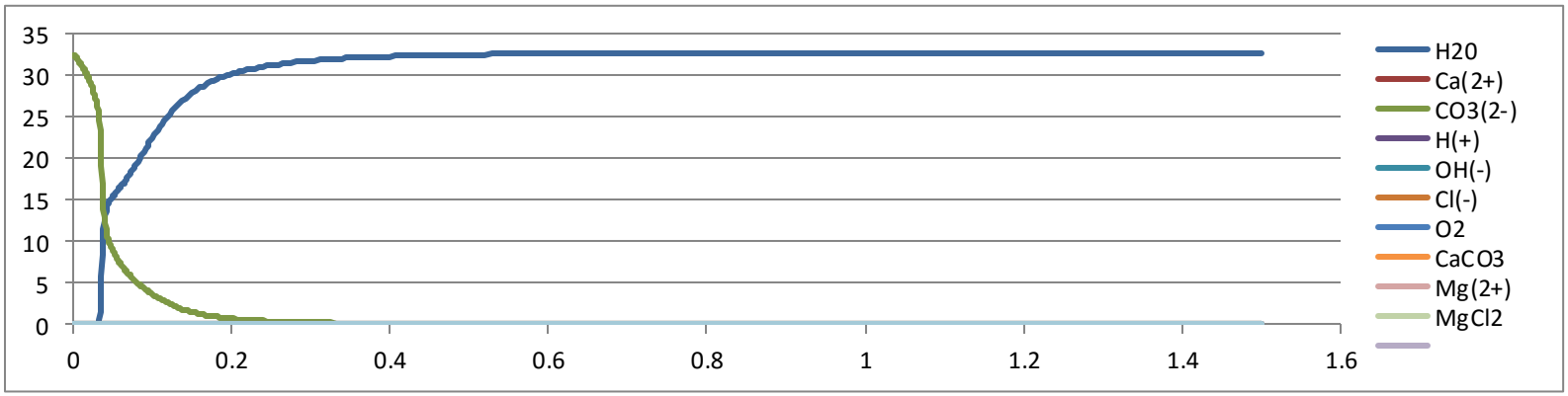

Fig 3.12: Concentration of components vs Distance from the Electrode at 1.5 V (Major Components)

CO_3^{2-} ion concentration on metal surface further increases and still dominant factor compared to other anions. OH^- concentration increases further to 0.08 part/nm^3. Water is thrown off the metal surface.

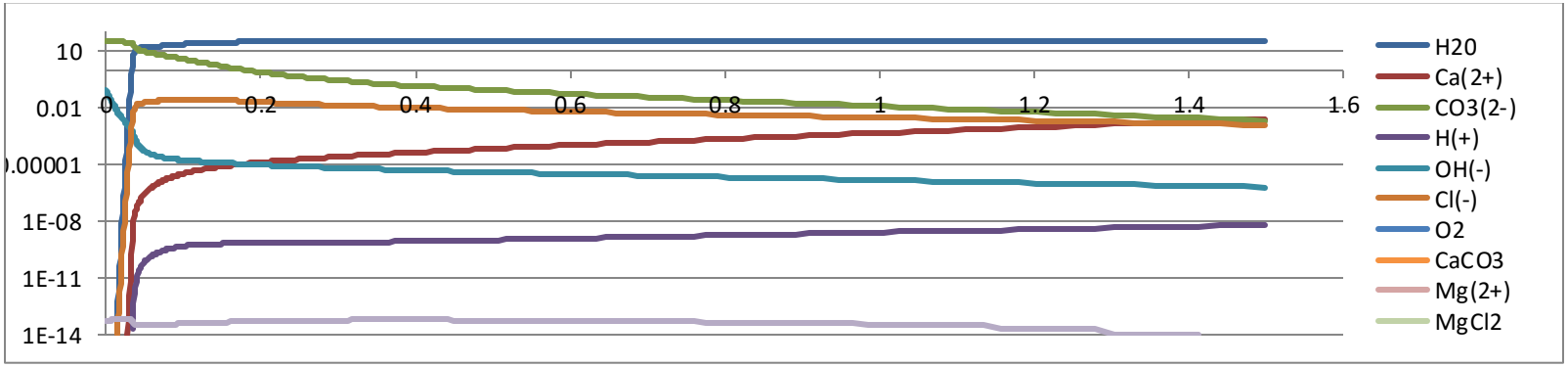

Fig 3.13: Concentration of components vs Distance from the Electrode at 1.5 V (Other Components in smaller quantities)

At 2V

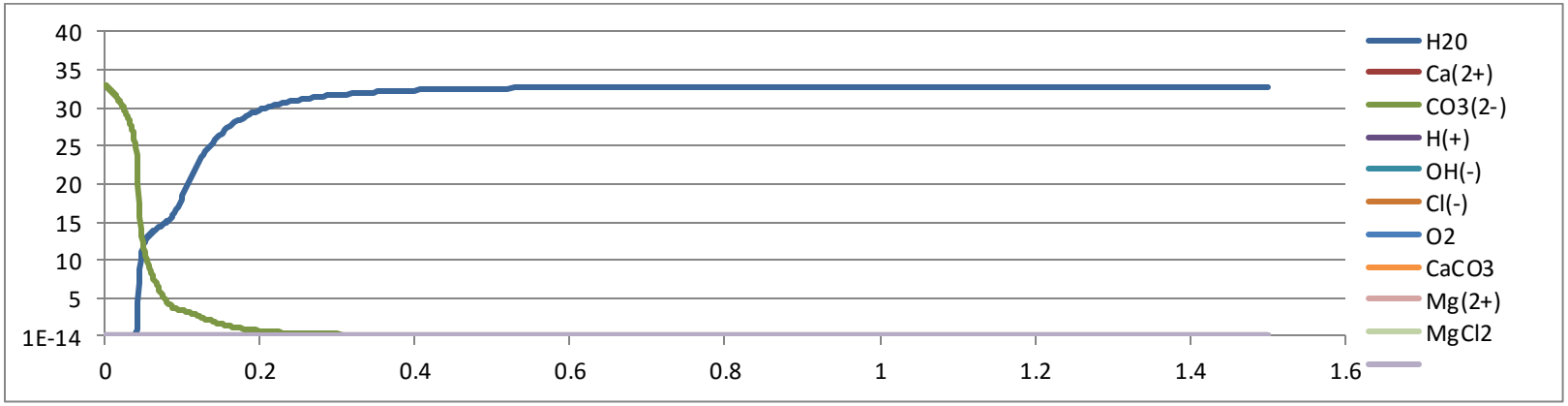

Fig 3.14: Concentration of components vs Distance from the Electrode at 2 V (Major Components)

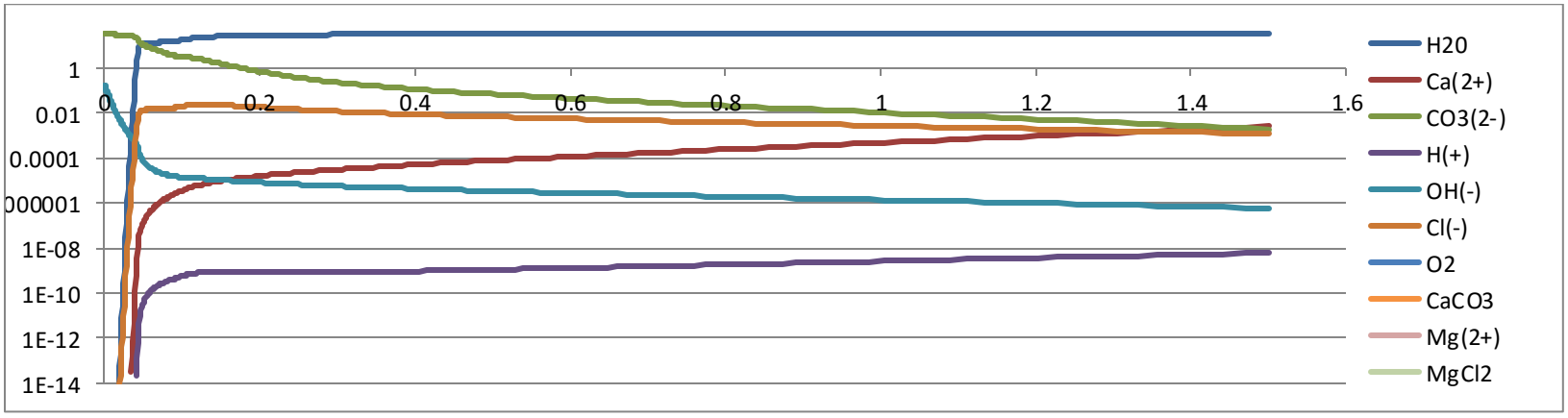

Fig 3.15: Concentration of components vs Distance from the Electrode at 1.5 V (Other Components in smaller quantities)

Assessing the plots of Concentration of components vs Distance from the metal surface, it can be observed that $CO3^{2-}$ is the dominant anion responsible for corrosion in our system.

It can be seen that as voltage increases from 0 to 2 V, concentration of $CO3^{2-}$ ions keeps on increasing towards the metal surface while other anion concentration remains considerably low.

At the same time, concentration of water on the metal surface is higher than $CO3^{2-}$ at low voltages. But this trend can be seen changing as we increase the voltage. Water concentration on metal surface decreases with increasing voltage. At higher voltage, water is eventually thrown of the metal surface.

Other anions like OH^-, Cl^- have relatively low concentration on the metal surface. OH^- ion concentration increases as the voltage is increased. Cl^- concentration on the surface of the metal reduces and is eventually thrown off the metal surface.

Packing factor, velocity and pressure of ions are some of the key parameters to determine the EDL structure.

We have plotted and analyzed the graphs for packing fraction, velocity and pressure of the ions with respect to distance from the metal surface.

3.2.1.2 Packing fraction vs Distance from Electrode

Packing fraction is basically the ratio of volume of set of objects to the total volume of the space. In our case, it signifies the density of the ions. A higher packing fraction would suggest that the ions are densely packed.

Here are plots of Packing Fraction vs Distance at different voltages.

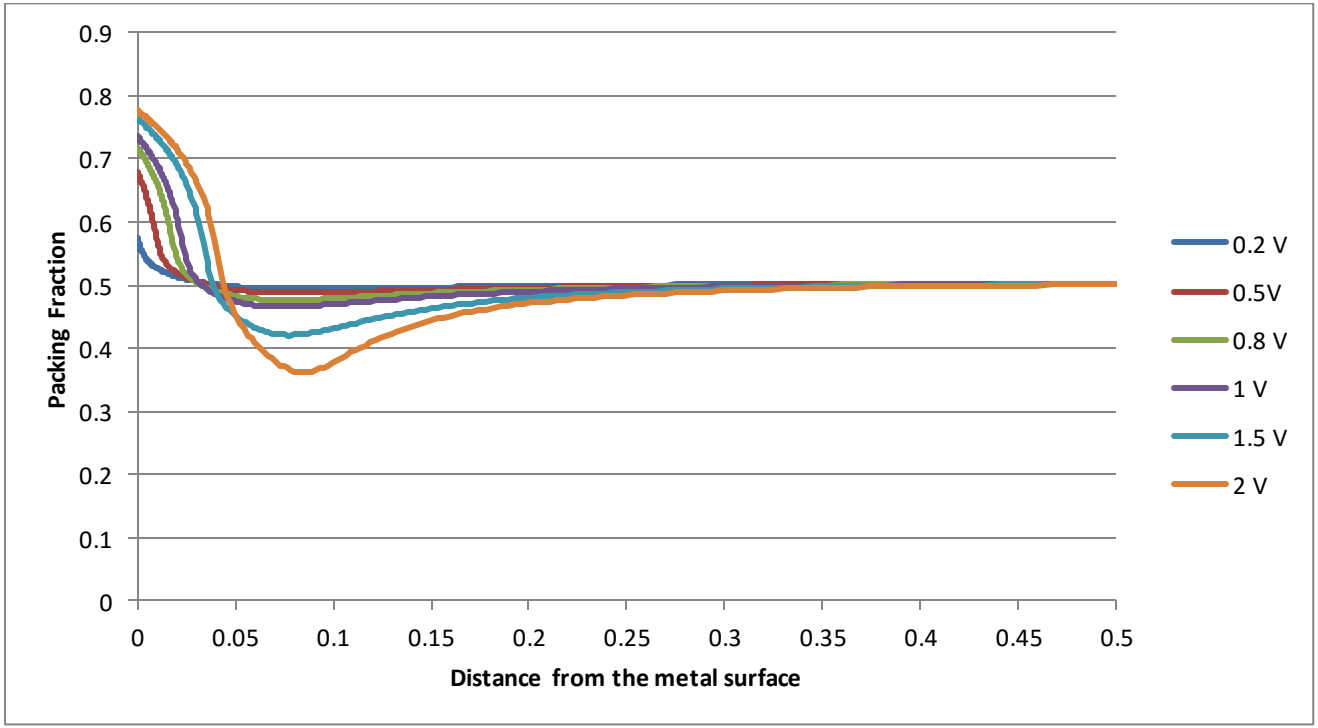

Fig 3.16: Plots for Packing Fraction vs Distance from the Electrodes for all potentials at 300K without considering metallic flux

Natures of the plots for Packing Fraction vs Distance remain same for different voltages. Packing fraction is maximum on the metal surface which shows density of ions is maximum on the metal surface and decreases gradually to minimum value at a certain distance from the metal surface. It increases exponentially to a constant value thereafter.

At 0.2 V, we can see that the packing fraction is maximum (0.585) at the metal surface and gradually decreases to a minimum value of 0.503 at 0.07 nm from the metal surface.

At 0.5 V, value of packing fraction at the surface of metal is 0.7. It decreases gradually to a minimum value of 0.497 at 0.07 nm from the surface of the metal and later increases to a constant value of 0.513 towards the electrolyte.

Packing fraction at the surface at 0.8V is 0.733 which gradually drops to 0.5026 at 0.096nm from the metal surface. It increases exponentially to 0.513.

At 1V, maximum packing fraction of 0.74 decreases to 0.4731 at 0.07 nm from the metal surface and increases thereafter.

Packing fraction at 1.5 V is 0.769 at the metal surface and decreases gradually to 0.4243 at 0.075nm from the surface and then increases to 0.513 towards the end.

At higher voltage of 2V, maximum value of packing fraction increases to 0.78 and decreases to a minimum value of 0.3383 at 0.08nm from the surface of the metal before it increases till 0.513

3.2.1.3 Velocity of ions vs Distance from Electrodes

We plot the graphs for Velocity of the ions vs Distance to analyze its effect on the Double Layer structure.

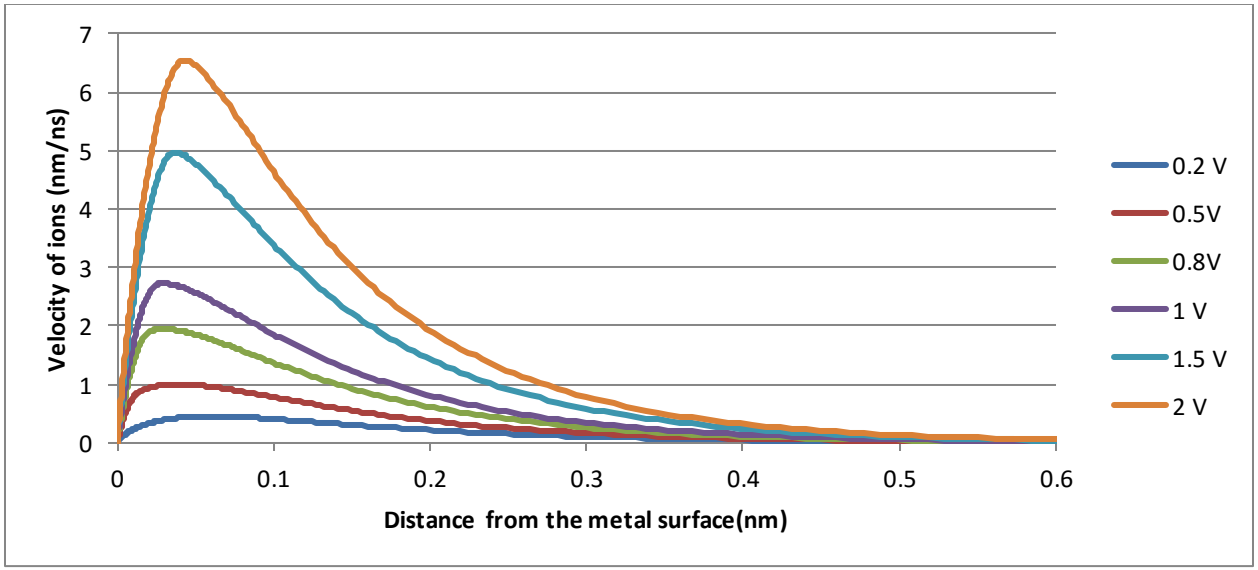

Fig 3.17: Plots for velocity of ions vs Distance from the electrode for all applied potentials at 300K without considering metallic flux

Observing the plots, it can be noticed that the ions are stationary on the metal surface. Velocities of the ions increase as they migrate from the surface to a peak value at some distance from the surface and gradually decrease and remain constant thereafter.

At 0.2 V, the velocity of the ions increases from the metal surface till it reaches a peak value of 0.46 nm/ns at 0.06 nm from the metal surface. Thereafter, it decreases as the ions diffuse.

At 0.5 V, velocity of ions which is minimum on the metal surface increases gradually to a maximum value of 1nm/ns at 0.04 nm from metal surface. Thereafter, it decreases and remains constant.

At 0.8 V, velocity of ions increases from the metal surface to a peak value of 1.948 nm/ns at 0.029 nm from the surface and decrease gradually later.

At 1 V, velocity of the ions increases as they move from the metal surface where velocity has a minimum value to a peak value of 2.72nm/ns at 0.03nm from the surface of the metal and decreases gradually after that to a constant value.

At 1.5 V, velocity of the ions increases from the metal surface as the start moving to a maximum value of 4.97 nm/ns at from the surface and decreases thereafter.

At 2V, velocity reaches a maximum value of 6.54 nm/ns at 0.043 nm from the metal surface and decreases later.

3.2.1.4 Pressure of ions vs Distance from Electrodes

Another important parameter in determination of EDL structure is the pressure of the ions. We have thus plotted for Pressure of the ions vs Distance from the surface.

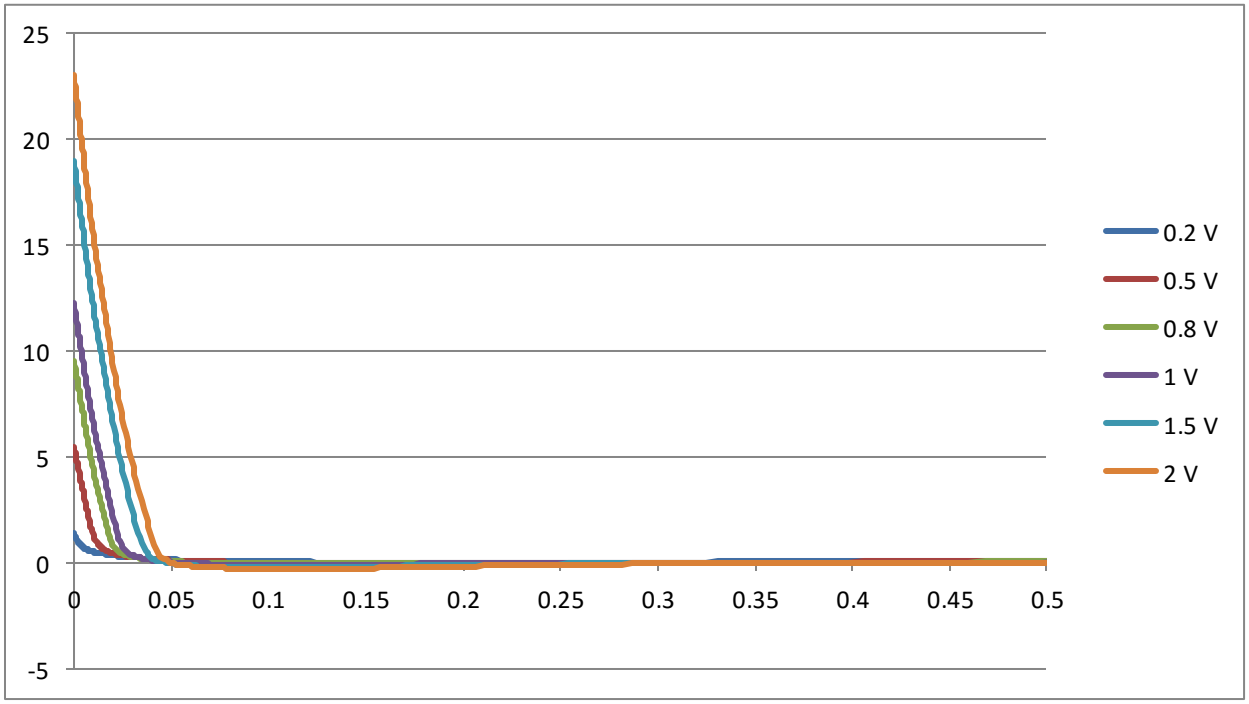

Fig 3.18: Pressure of the ions vs Distance from the Electrode at 300K without considering metallic flux

Pressure is maximum on the metal surface which steeply decreases to a negative minimum value and the pressure remains negative over a certain distance. Thereafter, it increases to remain constant in the bulk.

At 0.2 V, metal surface has the maximum pressure value of 1.47 GPa. Pressure decreases to a minimum value of -0.0115 GPa at 0.17nm from the metal surface. Pressure value remains negative from 0.109nm to 0.459nm from the metal surface.

Maximum pressure value on the metal surface is 5.55 Gpa which decreases to a minimum value of -0.3927 GPa at 0.13nm from the metal surface at 0.5V.

Pressure has a maximum value of 12.3 GPa on the metal surface and decreases to -0.1423 GPa at 0.1nm from the metal surface when the potential is 1V.

At 1.5 V, pressure at the metal surface is maximum at 19.03 GPa. It decreases till -0.277 GPa at 0.1nm from the surface and increases thereafter to 0.00157 GPa.

Pressure value on metal surface is maximum i.e. 23.06 GPa and drops till -0.346 GPa at 0.1 nm from the metal surface at 2V.

3.2.2 At 300K and Varying Electric Potenntial(considering metallic flux)

Metallic flux due to presence of metal ions on the surface is also an important dimension in determining the EDL structure. Metallic flux at a particular voltage can be determined using polarization curve for that metal. In our case, we consider the flux of Fe^{2+} ions as oxidation reaction of Fe at anode gives us Fe^{2+}. ($Fe = Fe^{2+} + 2e^{-}$)

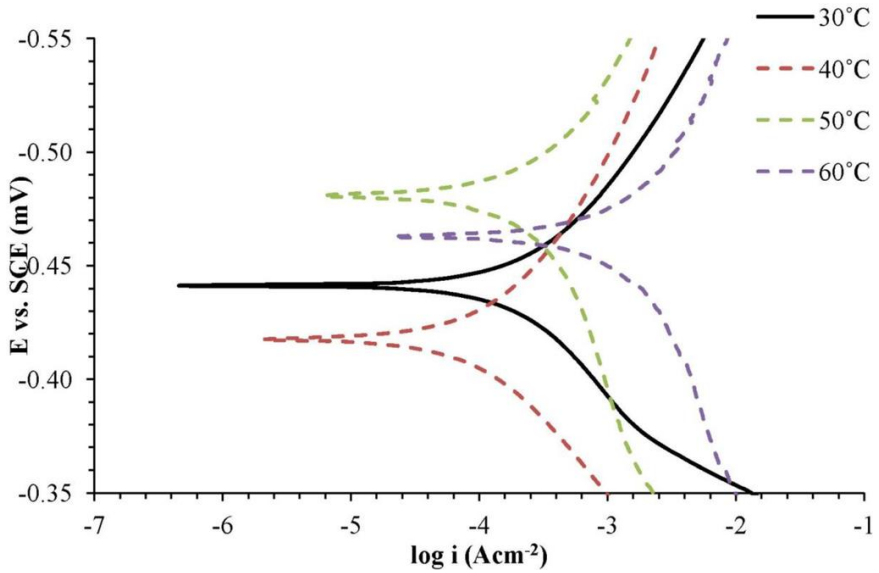

Fig 3.19: Polarization Curve of Stainless Steel [19]

3.2.2.1 Concentration of the components vs Distances from the Electrode

We first run the analytical model to study the concentration of components on the EDL surface.

At 0.2 V applying a flux of 6.25e-9 e/nm^2/ns

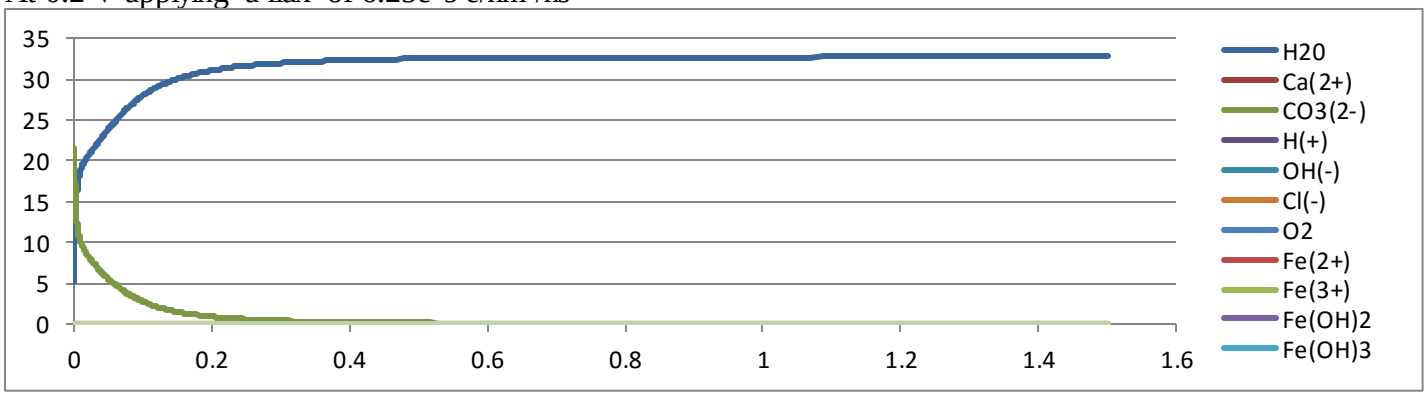

Fig 3.20: Concentration of components vs Distance from the Electrode at 0.2 V(considering flux) (Major Components)

CO_3^{2-} ions concentration is the dominating factor on the metal surface. Water concentration is low on the metal surface. Other anions are present in lower concentration on the surface. We can see the profile of concentration of components is exactly same as that for 0.2 V without considering flux.

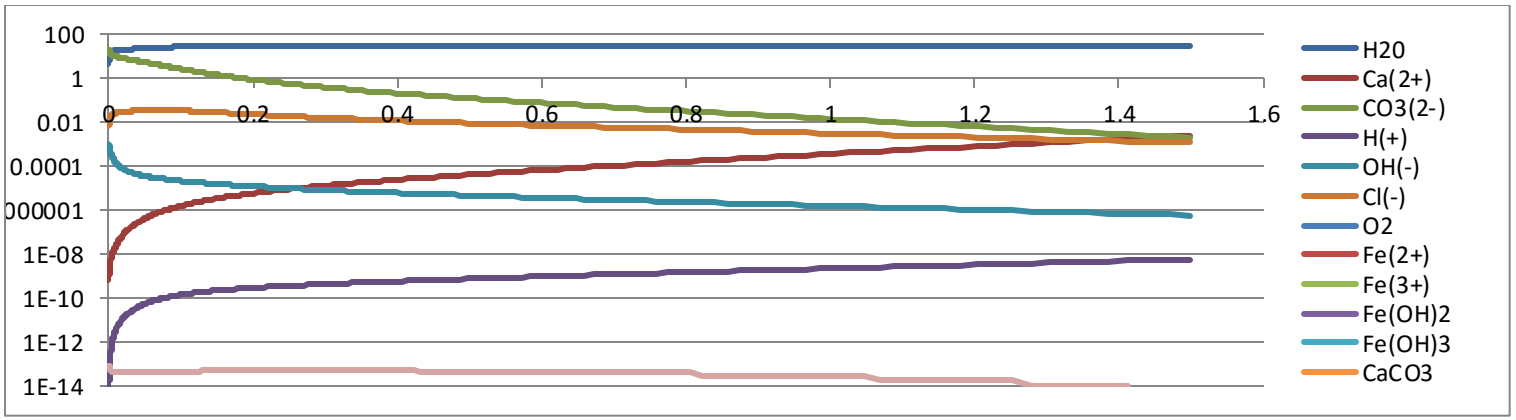

Fig 3.21: Concentration of components vs Distance from the Electrode at 0.2 V (considering flux) (Other Components in smaller quantities)

At 0.8 V applying a flux of 5.83e-8 e/nm^2/ns

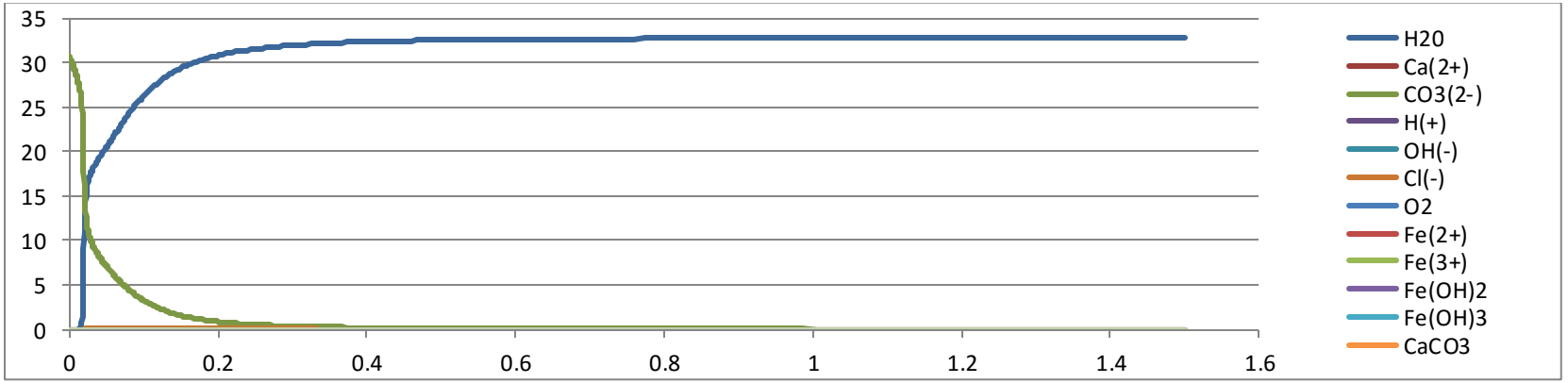

Fig 3.22: Concentration of components vs Distance from the Electrode at 0.8 V(considering flux) (Major Components)

CO_3^{2-} concentration still dominating the metal surface increases further to 30.64 part/nm^3. Other anions such as OH^- ,Cl^- are shown in the detailed plot below. OH^- increases to 0.01 part/nm^3 and Cl^- is further reduced from the surface. We can notice that concentration profile of components is exactly similar to what we had for 0.8V without applying any flux.

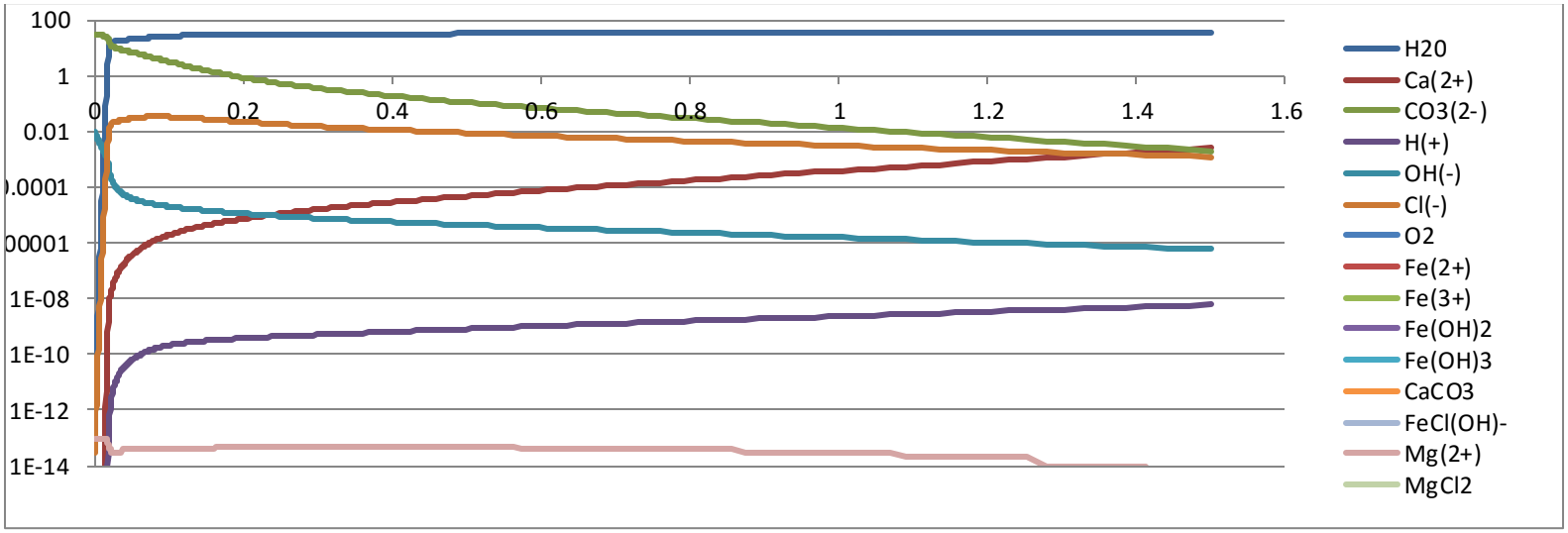

Fig 3.23: Concentration of components vs Distance from the Electrode at 0.8 V (Other Components in smaller quantities)

At 1.5 V applying a flux of 3.85e-6 e/nm^2/ns

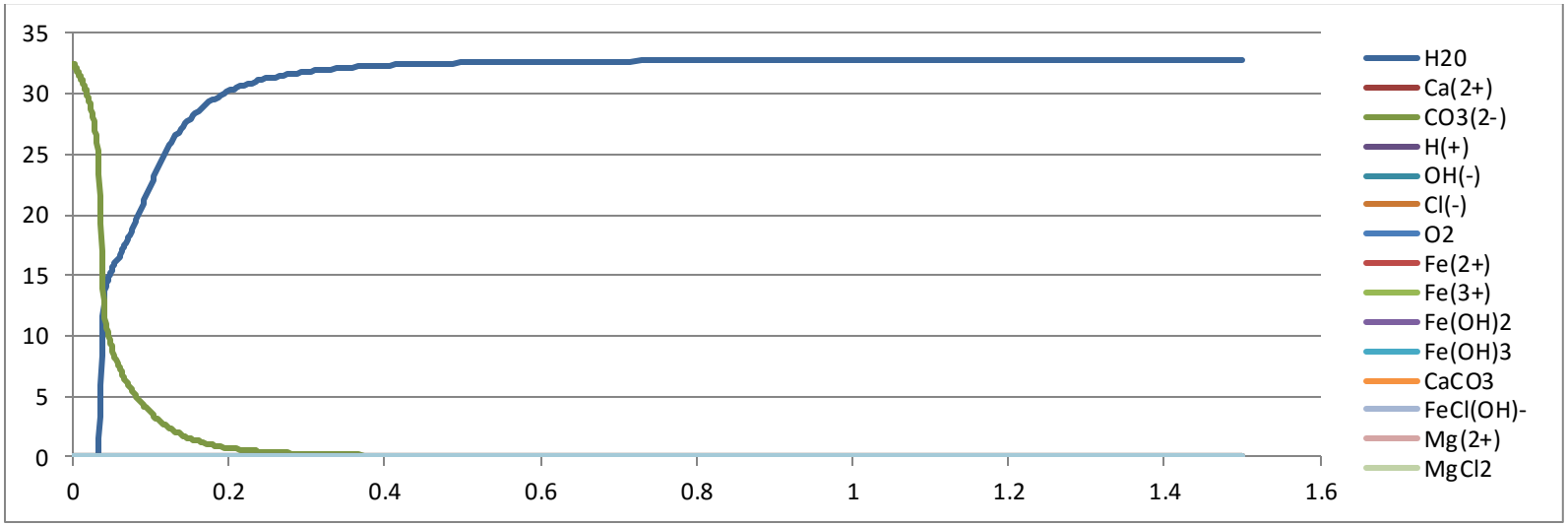

Fig 3.24: Concentration of components vs Distance from the Electrode at 1.5 V(considering flux) (Major Components)

At this voltage, CO_3^{2-} concentration on the surface further increases to 32.52 part/nm^3. OH^- concentration also increases to 0.08 part/nm^3. Cl^- and H_2O are thrown off the metal surface. An important observation is that the profiles for concentration is same as that we had for 1.5 V without applying any flux.

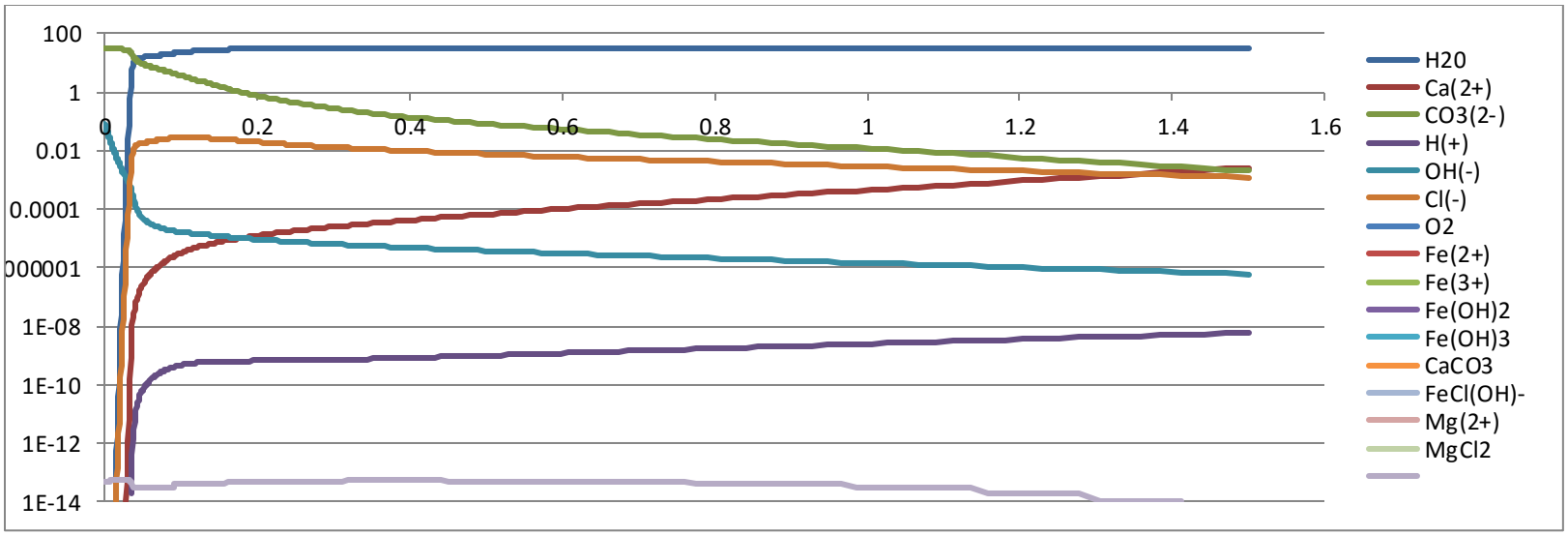

Fig 3.25: Concentration of components vs Distance from the Electrode at 1.5 V (Other Components in smaller quantities)

At 2V applying a flux of 6.85e-6 e/nm^2/ns

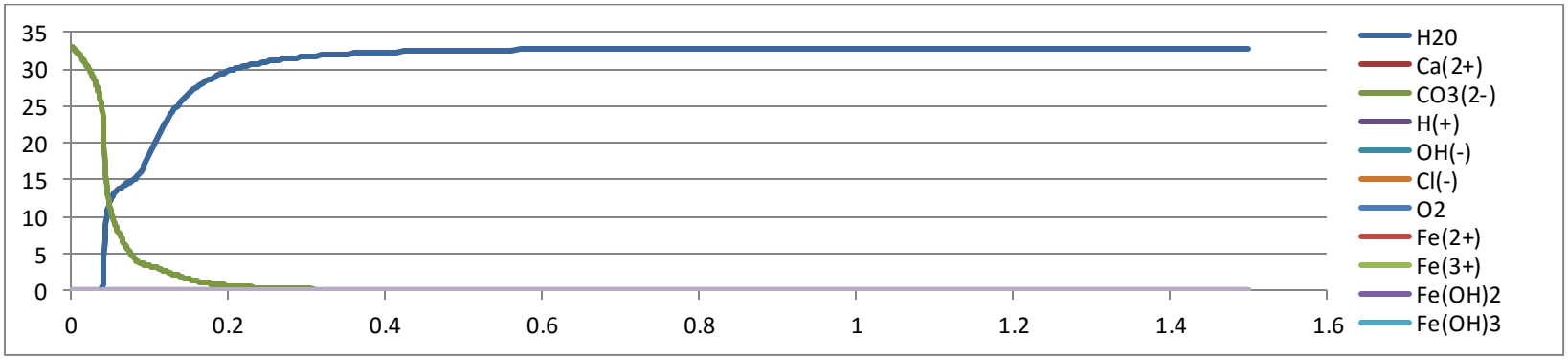

Fig 3.26: Concentration of components vs Distance from the Electrode at 2 V (considering flux) (Major Components)

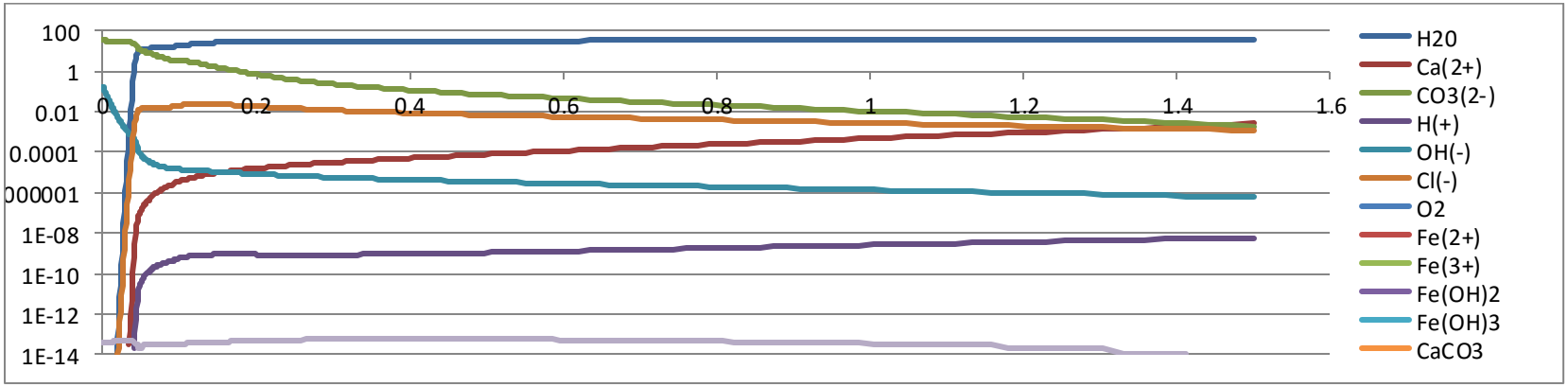

Fig 3.27: Concentration of components vs Distance from the Electrode at 2 V (considering flux) (Other Components in smaller quantities)

Carbonate anion is the only dominant factor in our system present on the metal surface causing corrosion. CO_3^{2-} ion concentration on the surface of the metal surface increases with increasing voltage. It can be seen that not only the nature of the graphs, but also the concentration of CO_3^{2-} ions and water molecules over the Double Layer are exactly same as they were in the earlier case when metallic flux was not considered.

It is not just that the concentration of ions on the DL surface remain same but the profiles of packing factor, velocity of the ions and the pressure of the ions also remain same as they were when we did not consider the flux due to metal ions as shown below.

3.2.2.2 Packing Fraction vs Distance from Electrode

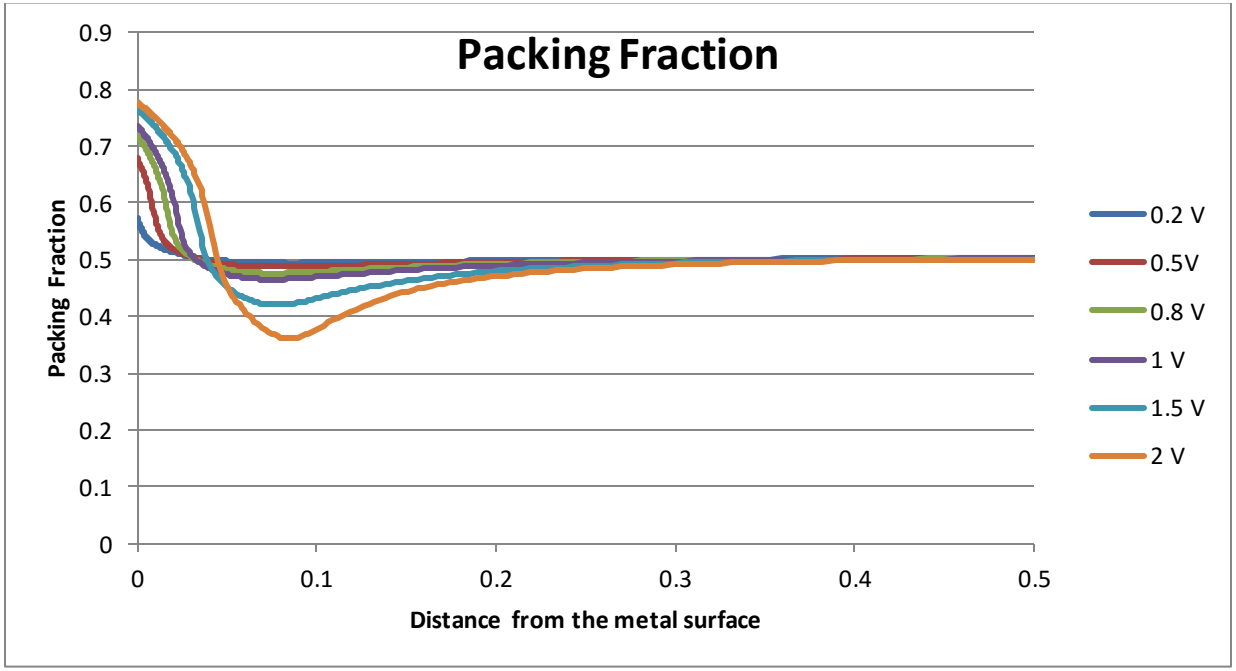

Figure 3.28: Packing Fraction vs Distance from Electrode at 300K considering flux

3.2.2.3 Velocity of ions vs Distance from Electrode

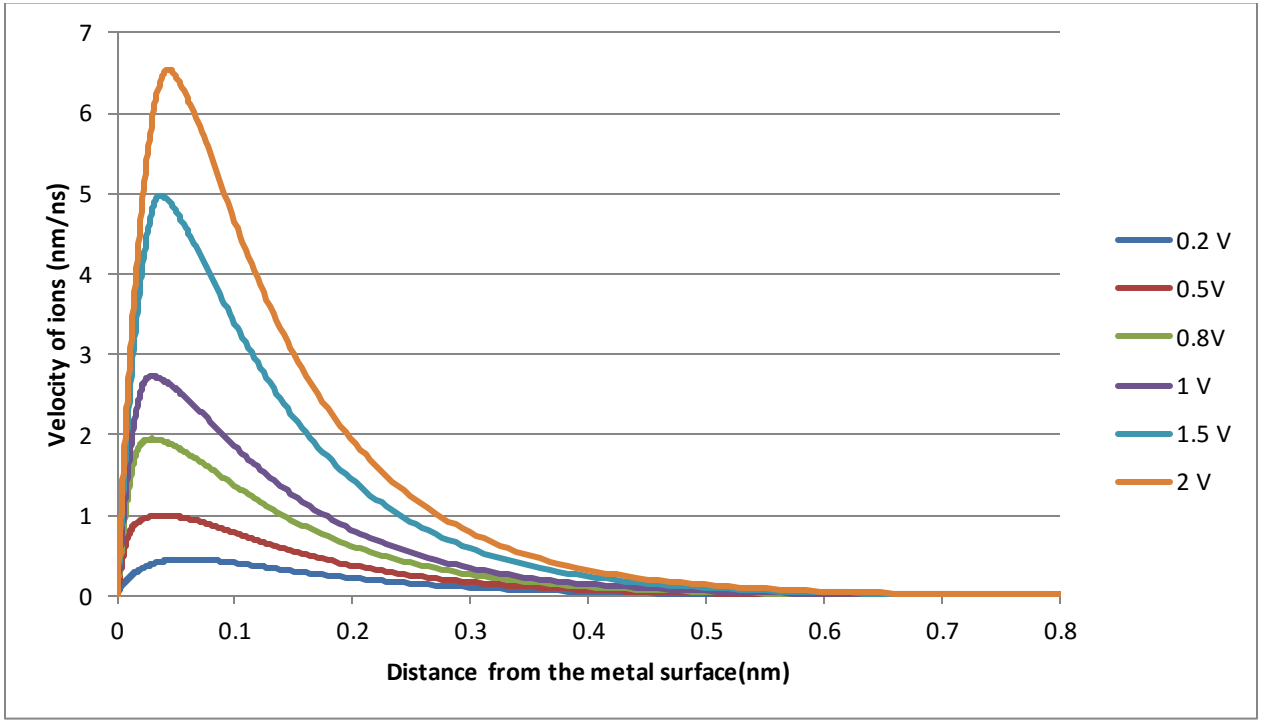

Fig 3.29: Velocity of ions vs Distance from Electrode at 300K considering flux

3.2.2.4 Pressure of ions vs Distance from Electrode

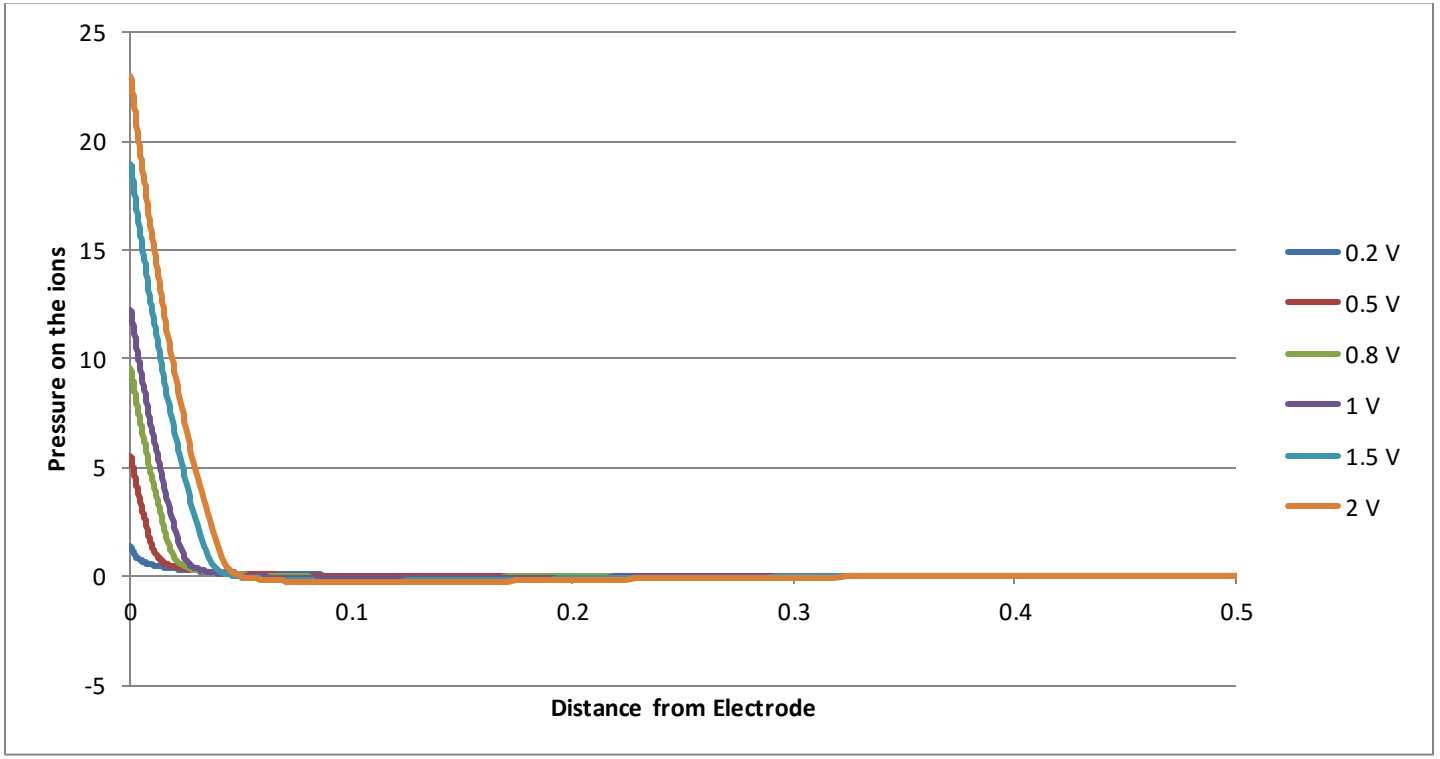

Fig 3.30: Pressure on the ions vs Distance from Electrode at 300K considering flux

3.2.3 At 323K Varying Voltage

Increasing the temperature of our system from 300 to 323 K for different electric potentials, we initially plot and analyze the concentration of components on the double layer.

3.2.3.1 Concentration of Components vs Distance from Electrode

At 0.2V

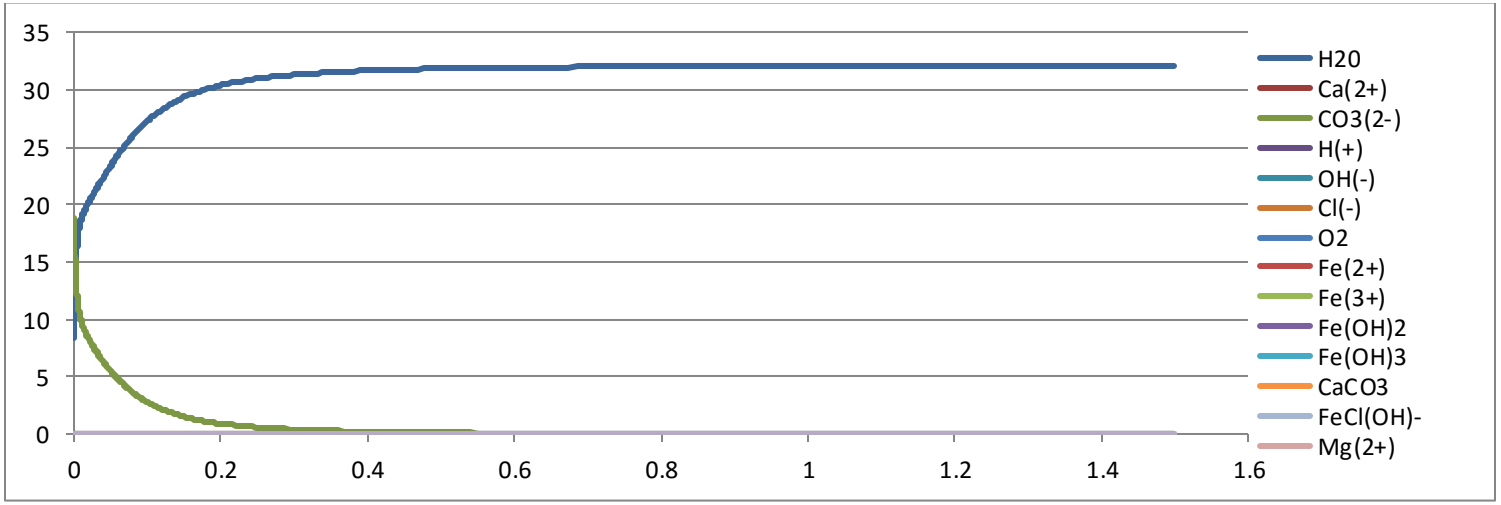

Fig 3.31: Concentration of components vs Distance from the Electrode at 0.2 V at 323K (Major Components)

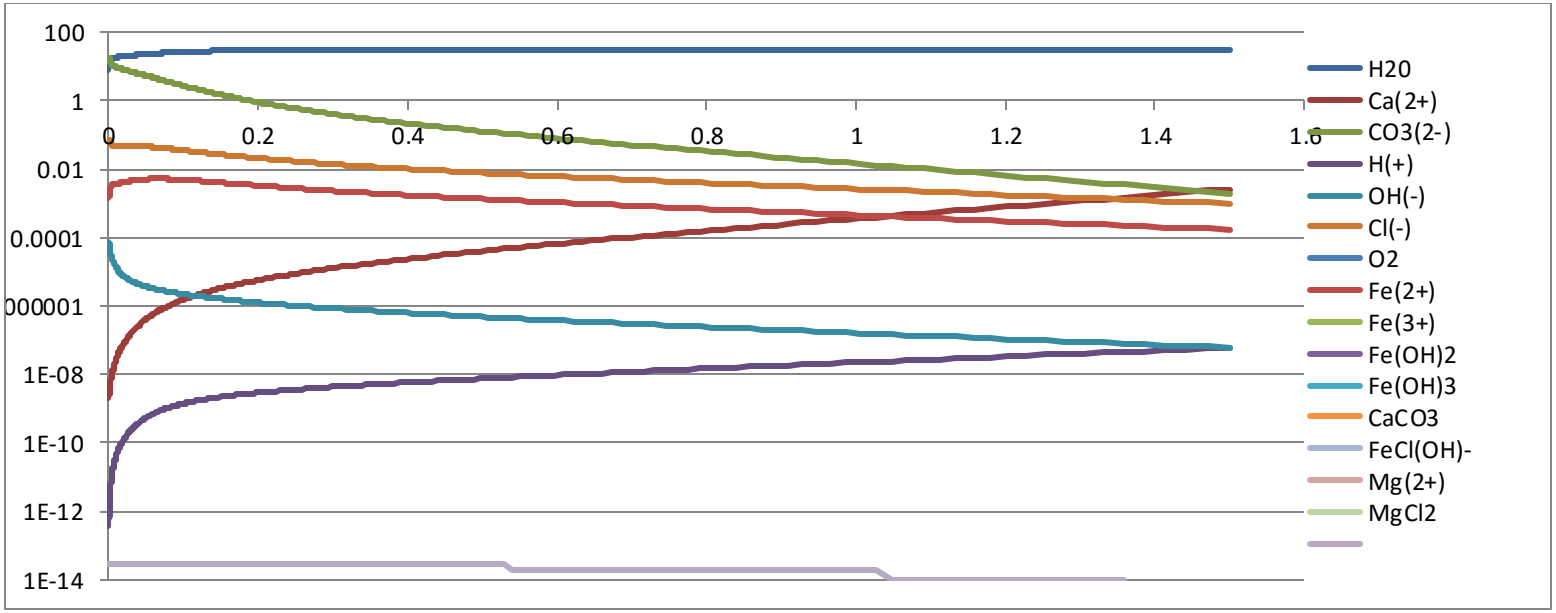

Fig 3.32: Concentration of components vs Distance from the Electrode at 0.2 V at 323 K (Other Components in smaller quantities)

At 0.5 V

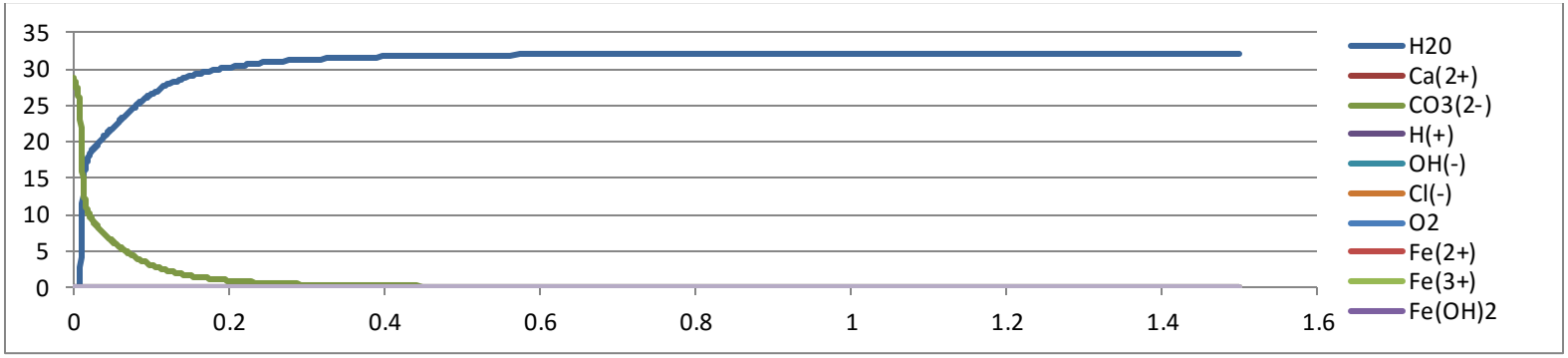

Fig 3.33: Concentration of components vs Distance from the Electrode at 0.5 V at 323K (Major Components)

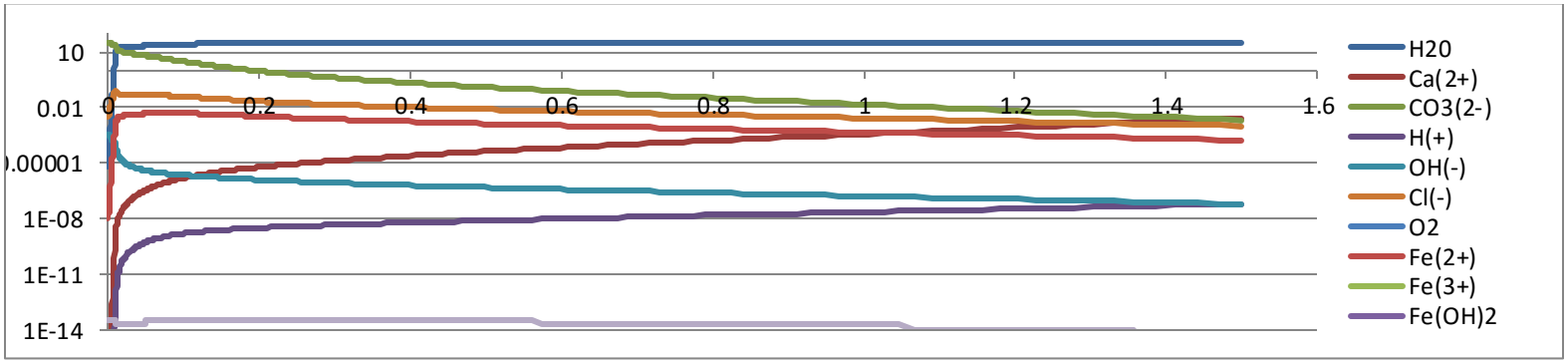

Fig 3.34: Concentration of components vs Distance from the Electrode at 0.5 V at 323 K (Other Components in smaller quantities)

At 0.8V

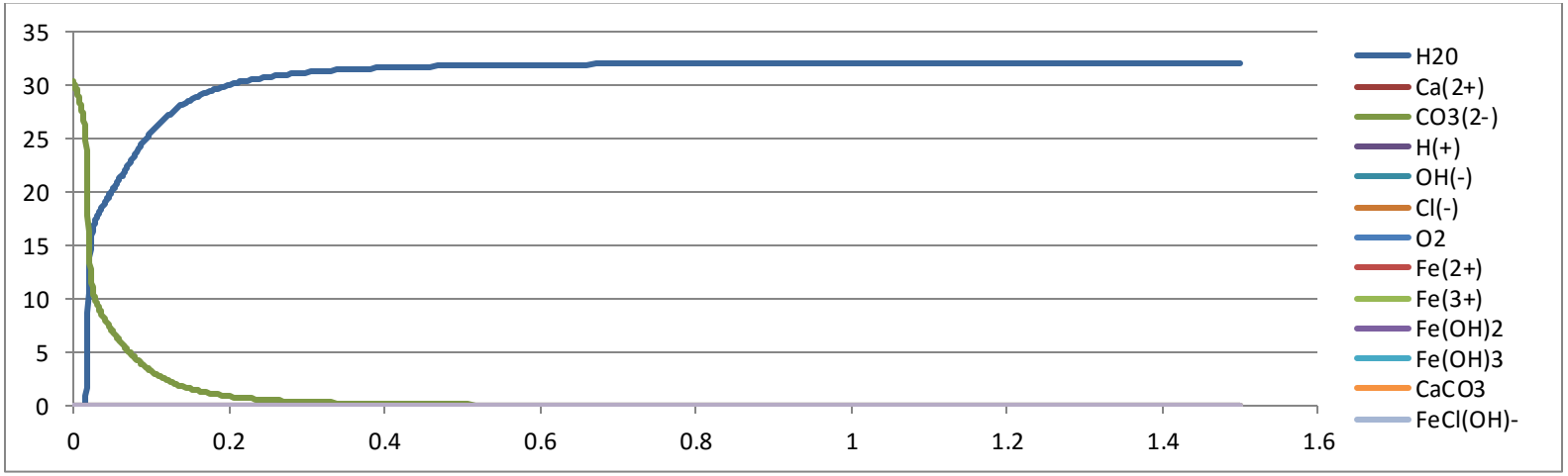

Fig 3.35: Concentration of components vs Distance from the Electrode at 0.8 V at 323K (Major Components)

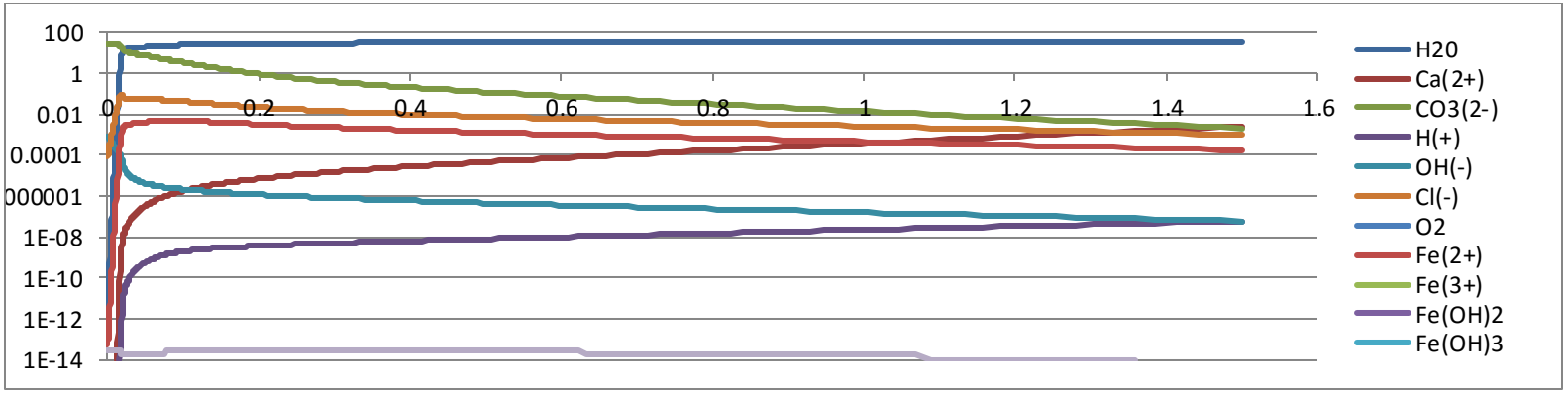

Fig 3.36: Concentration of components vs Distance from the Electrode at 0.8 V at 323 K (Other Components in smaller quantities)

At 1V

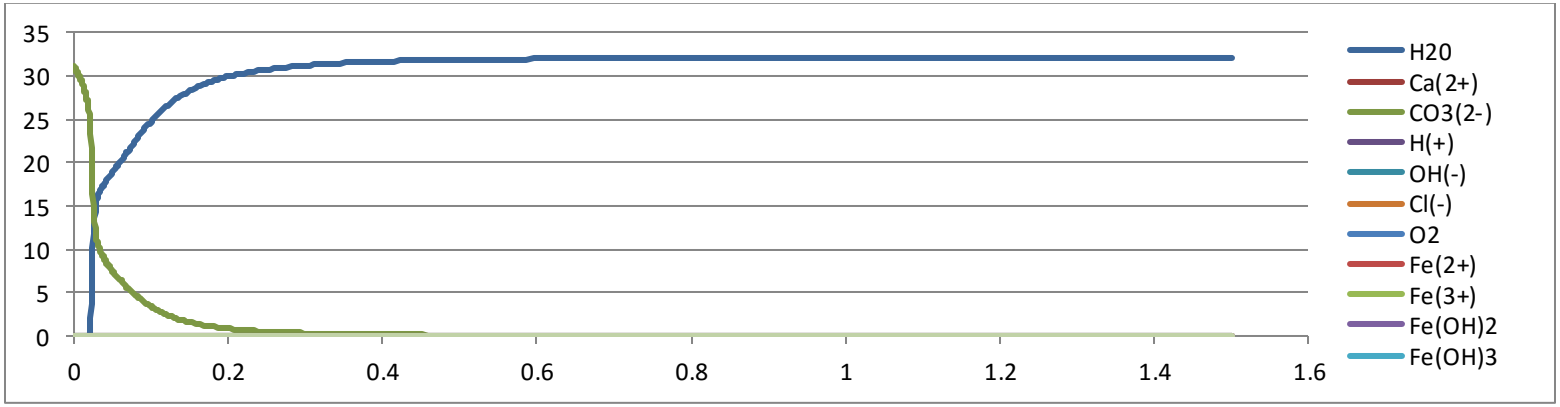

Fig 3.37: Concentration of components vs Distance from the Electrode at 1 V at 323K (Major Components)

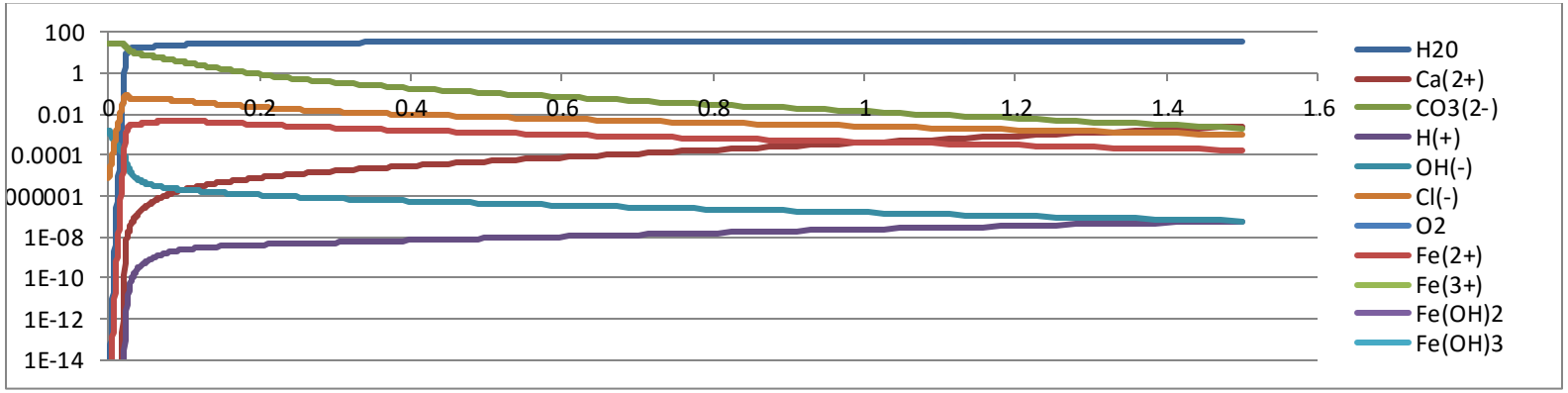

Fig 3.38: Concentration of components vs Distance from the Electrode at 1 V at 323 K (Other Components in smaller quantities)

At 1.5V

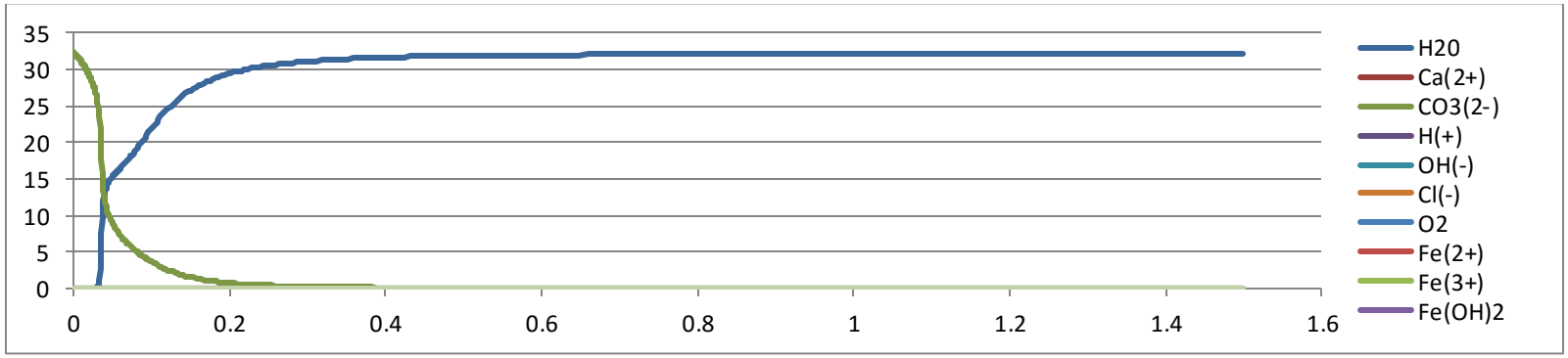

Fig 3.39: Concentration of components vs Distance from the Electrode at 1.5 V at 323K (Major Components)

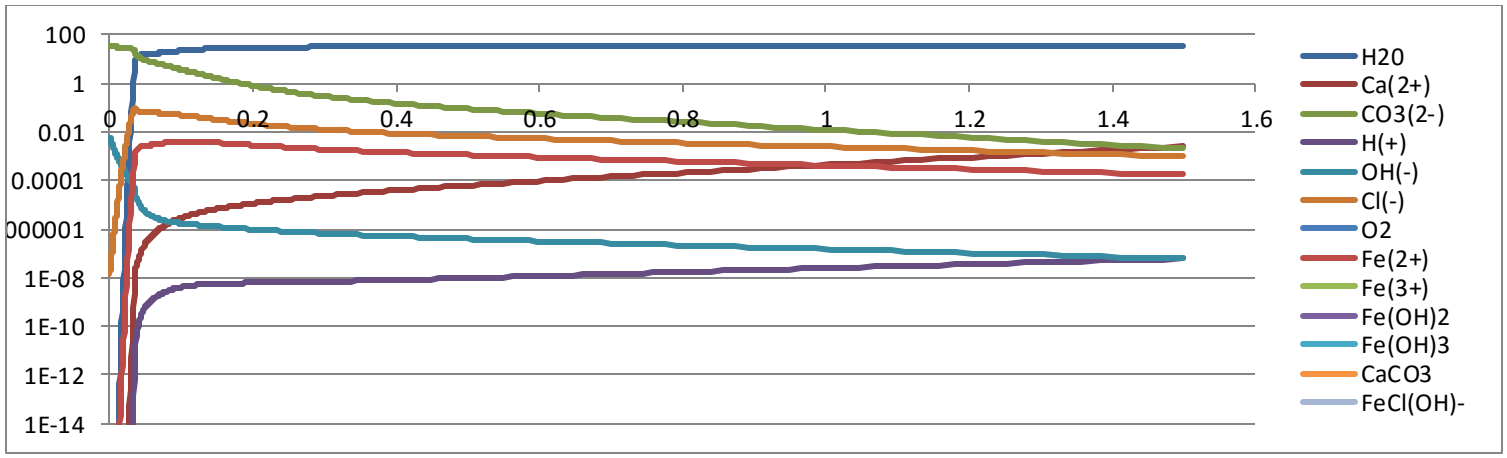

Fig 3.40: Concentration of components vs Distance from the Electrode at 1.5 V at 323 K (Other Components in smaller quantities)

At 2V

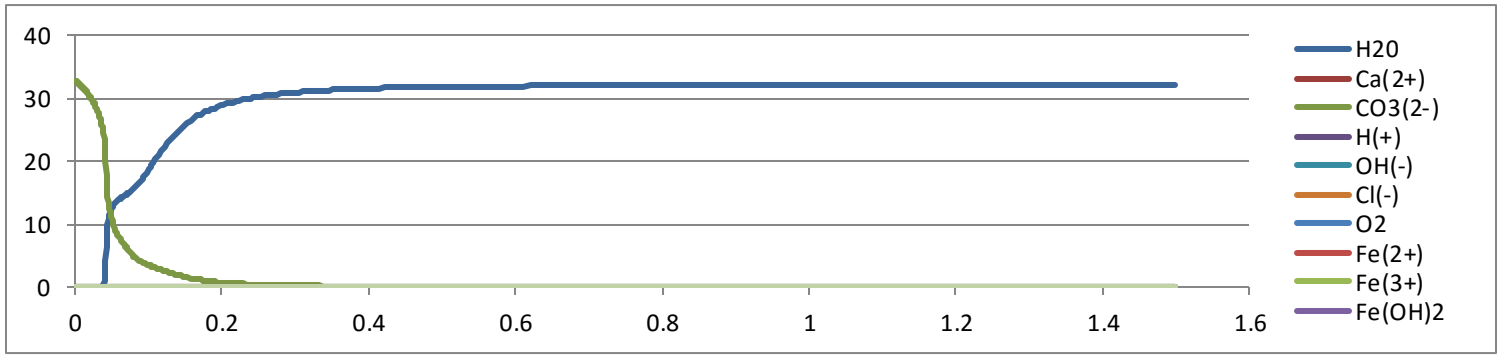

Fig 3.41: Concentration of components vs Distance from the Electrode at 2 V at 323K (Major Components)

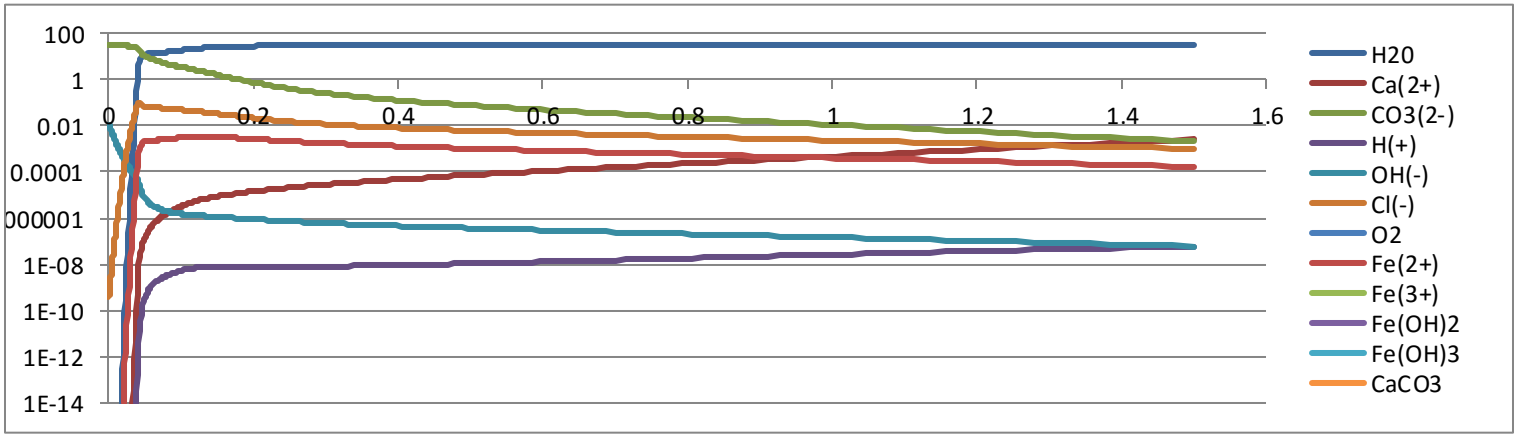

Fig 3.42: Concentration of components vs Distance from the Electrode at 2 V at 323 K (Other Components in smaller quantities)

Even after varying the temperature, carbonate ions continue to dominate the surface of the metal. As the voltage increases, CO_3^{2-} ion concentration on the metal surface increases and concentration of water on the metal surface decreases and eventually gets thrown off the surface. These observations are similar to the earlier case at 300 K. But it can be noted at lower voltages at higher temperature, there is a decrease in concentration of CO_3^{2-} ions on the surface of the metal compared to the concentration at 300K.

Profiles for Packing Fraction, Velocity of ions and Pressure of the ions have also been plotted and studied with respect to distance from the metal surface as shown below.

3.2.3.2 Packing Fraction vs Distance from Electrode (At 323K)

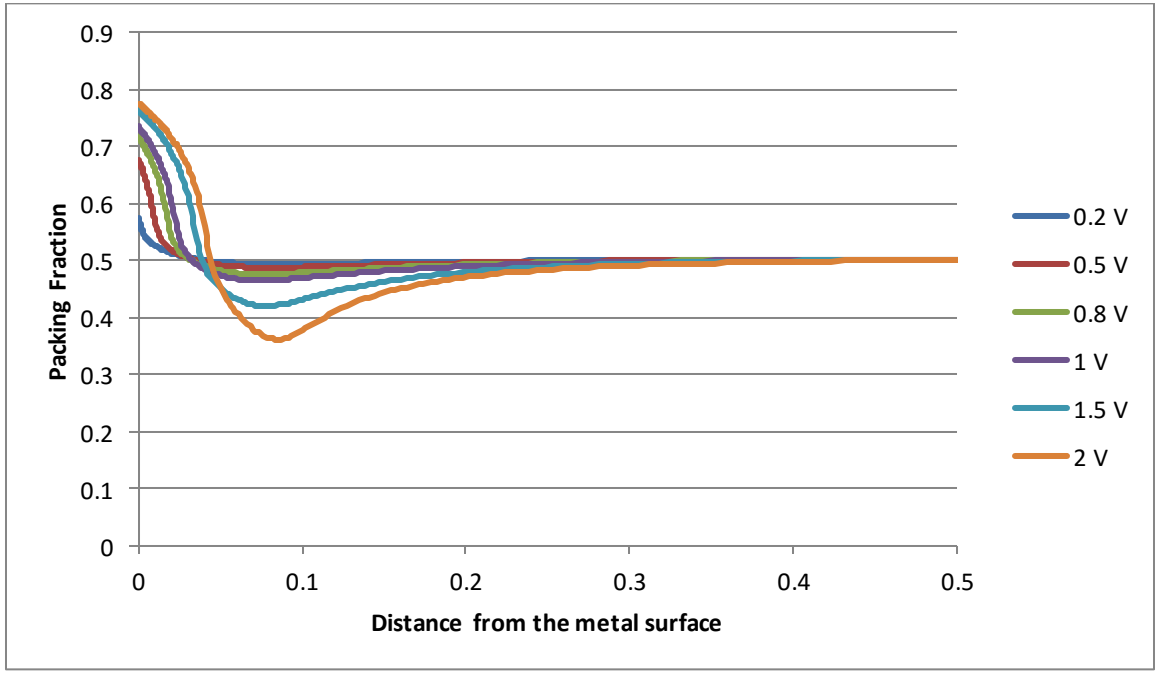

Fig 3.43: Packing Fraction vs Distance from Electrode at 323K

3.2.3.3 Velocity of ions vs Distance from Electrode

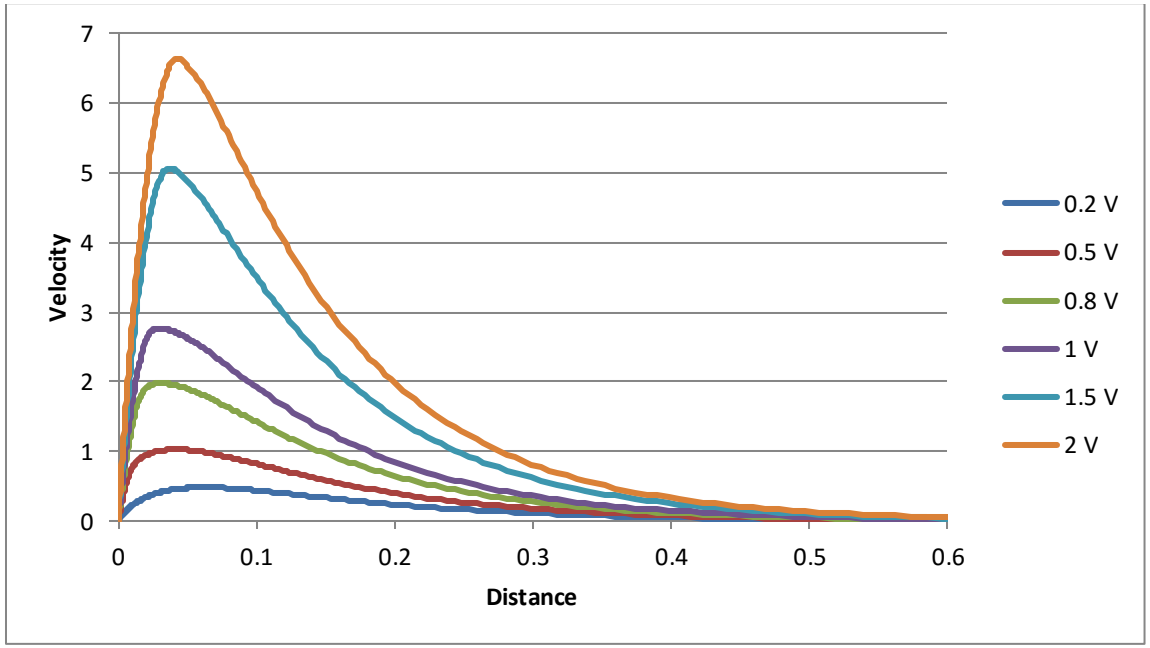

Fig 3.44: Velocity of the ions vs Distance from Electrode at 323K

3.2.3.4 Pressure on the ions vs Distance from Electrode

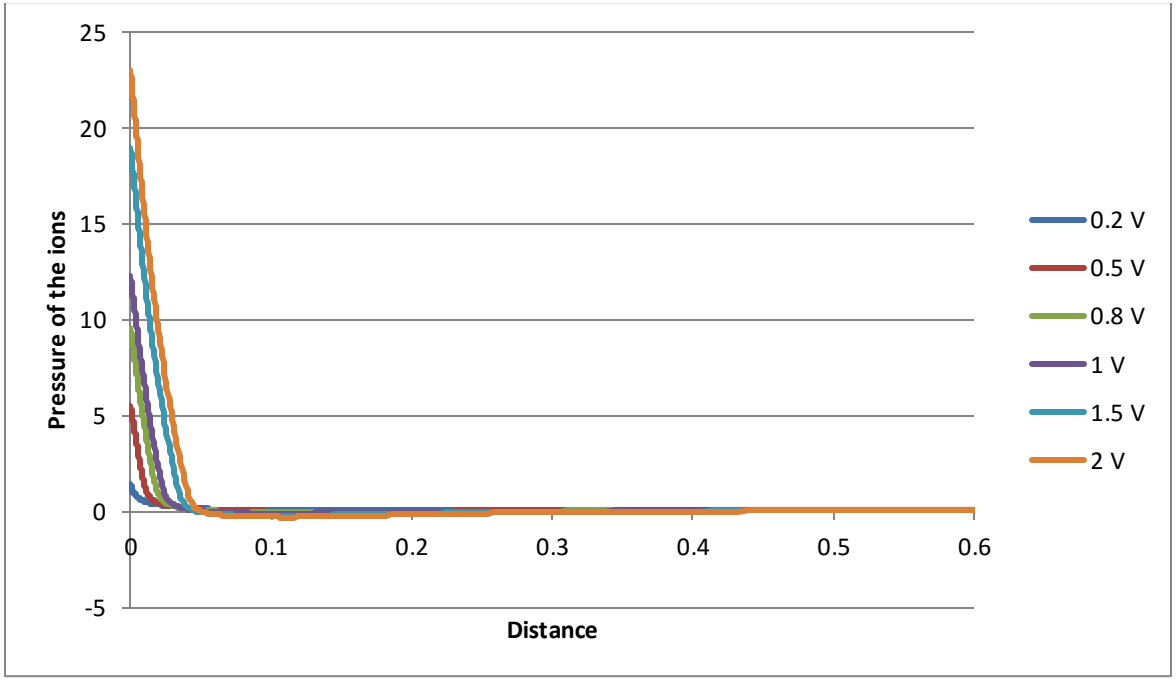

Fig 3.45: Pressure on the ions vs Distance from the Electrode at 323K

After observing these plots, it can be noticed that the nature of the plots for packing fraction, velocity and pressure of the ions are similar to that what they were for 300 K.

Chapter 4

Conclusion

In the previous section, using the analytical simulation model we achieved the plots for Concentration of components vs Distance, Packing Fraction vs Distance, Pressure vs Distance and Velocity of ions vs Distance for different voltages and temperatures.

Observing the plots for Concentration vs Distance, it can be clearly seen that CO3(2-) is the only dominant factor in initiating the corrosion process. But, concentration of this dominant factor on the surface of metal varies with respect to electric potential applied. We can see the concentration of CO3(2-) on the metal surface increases with increase in voltage. It can thus be inferred that more anions are attracted towards the metal surface as the electric potential applied through the system increases. This is mainly due to the formation of Fe^{2+} ions on the metal surface as a result of oxidation of Fe which attracts more counter anions like CO_3^{2-} to the surface. For different temperature at 323K, the nature of the plots and results remain same i.e. single dominant anion. However, it can be noticed that for a given voltage, concentration of CO3 (2-) ion on the metal surface is

lightly less as compared to that at lesser temperature(300 K). We can also notice that concentration of water (H2O) on the metal surface decreases as the electric potential increases and eventually gets thrown off the surface of the metal at higher voltages.

By studying the graphs for Packing Fraction vs Distance, it can be seen that natures of the plots remain similar for different voltages and temperatures. At the metal surface, packing fraction has a maximum value which decreases gradually to a minimum value at a certain distance from the metal surface and increases exponentially thereafter. Thus we can infer that density of the ions is maximum at the metal surface. This is generally due to the presence of the metal ions and counter anions on the metal surface. This reduces gradually till a certain distance from the surface before the density starts increasing. As the voltage increase, density of ions on the metal surface increase. Thus we see packing fraction on the metal surface increases with voltage. As temperature increases to 323 K, there is no significant change in the density however, it can be seen that there is a slight decrease in the packing fraction on the surface which shows us that density of ions decrease with increase in temperature.

As we notice the plots for Velocity of ions vs Distance, it can be observed that ions are nearly stationary at the surface due to high density of ions on the metal surface. They start moving rapidly till they achieve a peak velocity at a certain distance from the surface of the metal before they start decreasing the velocity. It can be seen that this peak velocity increases with rise in voltage and the distance at which they achieve this velocity decreases with rising voltage. Thus it can be concluded that the ions start moving faster as voltage rises. For an increase it temperature at the same voltage, we see that the value of peak velocity reduces slightly.

The plots for Pressure exerted by the ions vs Distance from the metal surface maintain a similar nature even after varying voltage and temperature. Pressure is maximum on the metal surface which drops to a minimum negative value at a certain distance from the metal surface. Thereafter, it slightly increases to a definite positive value. Pressure remains negative for a certain distance after it decreases. Negative pressure zone is due to the vaporization of the electrolyte.

Looking at the results, it can said that electric potential is a very important parameter in the corrosion process having many effects on the Double Layer Structure.

Appendix A

Input profile for our system at 300K varying potential from 0.2 to 2V in 20 steps

```
**********1D Problem******************
1              !=1 if planar; =2 if cylindrical; =3 if spherical
300            !Temperature(K)
**********Domain and Grid******************
0, 1.5, 250, 1.02       !XStt,XEnd(nm),Total # of divisions,Mesh-grading power
**********Involved Chemical Components*********
17      !Total#Of Involved Chemical Components
1, 2,3, 4, 5, 6, 7, 8, 9,10,12,14,15,16,18,19,20        !Above#X(ID_Glb Of Involved Chemical Component)
**********Involved Chemical Reactions*********
11      !Total#Of Involved Chemical Reactions
1,2,3,4,5,6,7,8,9,11,12,13,14,15        !Above#X(ID_Glb Of Involved Chemical Reaction)
**********Simulation Time & Steps**********************
20, 20          !NtotTimeSteps,NtotSnapShots
0               !ITimeStt(=0, first time run; >0, to restart based on ITimeStt-1 step)
**********Initial Uniform Concentrations**********************
32.76, 2.6d-3, 2.01d-3, 0.602d-7, 0.602d-7, 1.7d-4, 0, 0, 0,0,0,0,0,0,0, 0,0,0 !C(particle/nm^3)///MUST Follow the above order of involved chemical components
**********Boundary Condition*************
!---repeat below !NthC,Ramp1Jump2,2(Flux0_End,SpringCoef_End,C_Eqilibrium_End)
0, 1, 0, 1.d3, 2, 0, 1.d3, 0                    !electric (Displacement=Displacement0+Coef*(V-V0)) with displacement_unit:e/nm^2
1, 2, 0, 0, 0, 0, 1.d3, 32.76                   !chemical (flux=flux0+Coef*(C-C0)) with flux_unit:particle/nm^2/ns, and C_unit:particle/nm^3
2, 2, 0, 0, 0, 0, 1.d3, 2.6d-3                  !chemical (flux=flux0+Coef*(C-C0)) with flux_unit:particle/nm^2/ns, and C_unit:particle/nm^3
3, 2, 0, 0, 0, 0, 1.d3, 2.01d-3                 !chemical (flux=flux0+Coef*(C-C0)) with flux_unit:particle/nm^2/ns, and C_unit:particle/nm^3
4, 2, 0, 0, 0, 0, 1.d3, 0.602d-7                !chemical (flux=flux0+Coef*(C-C0)) with flux_unit:particle/nm^2/ns, and C_unit:particle/nm^3
5, 2, 0, 0, 0, 0, 1.d3, 0.602d-7                !chemical (flux=flux0+Coef*(C-C0)) with flux_unit:particle/nm^2/ns, and C_unit:particle/nm^3
6, 2, 0, 0, 0, 0, 1.d3, 1.2d-3
7, 2, 0, 0, 0, 0, 1.d3, 0                       !chemical (flux=flux0+Coef*(C-C0)) with flux_unit:particle/nm^2/ns, and C_unit:particle/nm^3
8, 2, 0, 0, 0, 0, 1.d3, 0                       !chemical (flux=flux0+Coef*(C-C0)) with flux_unit:particle/nm^2/ns, and C_unit:particle/nm^3
9, 2, 0, 0, 0, 0, 1.d3, 0                       !chemical (flux=flux0+Coef*(C-C0)) with flux_unit:particle/nm^2/ns, and C_unit:particle/nm^3
10, 2, 0, 0, 0, 0, 1.d3, 0                    !chemical (flux=flux0+Coef*(C-C0)) with flux_unit:particle/nm^2/ns, and C_unit:particle/nm^3
11, 2, 0, 0, 0, 0, 1.d3, 0                    !chemical (flux=flux0+Coef*(C-C0)) with flux_unit:particle/nm^2/ns, and C_unit:particle/nm^3
12, 2, 0, 0, 0, 0, 1.d3, 0                    !chemical (flux=flux0+Coef*(C-C0)) with flux_unit:particle/nm^2/ns, and C_unit:particle/nm^3
13, 2, 0, 0, 0, 0, 1.d3, 0                    !chemical (flux=flux0+Coef*(C-C0)) with flux_unit:particle/nm^2/ns, and C_unit:particle/nm^3
14, 2, 0, 0, 0, 0, 1.d3, 0                    !chemical (flux=flux0+Coef*(C-C0)) with flux_unit:particle/nm^2/ns, and C_unit:particle/nm^3
15, 2, 0, 0, 0, 0, 1.d3, 0
16, 2, 0, 0, 0, 0, 1.d3, 0
17, 2, 0, 0, 0, 0, 1.d3, 0
**********Numerical Parameters**********************
90000, 1.d-3, 1000, 0.0007      !IteratMax,ErrAllow,IteratDisplay,ARelax
*************************************************************************
**********All Chemical Components**********************
20      !Total # of chemical components
--repeat (above #) below--!ID;Valance;Relative_Permittivity@Linear;StokesRadius;PhysicalRadius;EtaOverEpsil0((V/nm)^2-nS);AvdW0
 1,  0,   79, 0.09687,   0.1552,  0.113d1, 0.20294                      !H2O(0)(10)
 2,  2,    3,  0.0344,    0.099,  0.113d1, 0.20294                      !Ca(2+)(40)
 3, -2,    2, 0.03086,    0.178,  0.113d1, 0.20294                      !CO3(2-)(17)
 4,  1,    0,  0.0244,   0.1552,  0.113d1, 0.20294                      !H(1+)(1):CInf_H+=0.602d-7(pH=7)
 5, -1, 64.4,  0.0431,    0.137,  0.113d1, 0.20294                      !OH(1-)(9):CInf_OH-=0.602d-7(pH=7)
 6,  -1,   10, 0.1082,    0.181,  0.113d1, 0.20294                      !Cl(1-)(17)
 7, 0, 6.89,   0.109,   0.135 , 0.113d1, 0.20294                       !O2(16)
 8,  2,  7.6,   0.311,    0.072, 0.113d1, 0.20294                       !Mg(2+)
 9,  2,   16,  0.3851,    0.06,  0.113d1, 0.20294                       !Fe(2+)(26)
10,  3, 15.8,  0.3861,   0.07,   0.113d1, 0.20294                       !Fe(3+)
 11,  0, 15.1,   0.213,    0.161, 0.113d1, 0.20294                      !HCl
 12,  1,   16,  0.3851,    0.126,  0.113d1, 0.20294                     !Fe
 13,  1, 14.2,   0.164,    0.216, 0.113d1, 0.20294                      !FeOH(+1)
 14,  0, 14.2,   0.165,   0.369,  0.113d1, 0.20294                      !Fe(OH)2
 15, 0, 14.2,   0.380,   0.382,  0.113d1, 0.20294                       !Fe(OH)3
16,  1, 13.8,  0.4613,   0.2246, 0.113d1, 0.20294                       !Fe(OH)Cl(1+)
 17,  2, 14.6,  0.4613,   0.2246, 0.113d1, 0.20294                      !FeCl(2+)
18,  1, 14.6,  0.4613,   0.2246, 0.113d1, 0.20294                       !FeCl2
19, 0,  9.1,   0.0344,   0.0348,  0.113d1, 0.20294                      !CaCO3
20,  1,  5.6,   0.311,   0.1847, 0.113d1, 0.20294                       !MgCl(1+)
**********All Chemical Reactions**********************
15      !Total # of Chemical Reactions
--repeat (above #) below--ID,KConst(MUST be consistent to generate rate by particle/nm^3/ns),4(NCLnr,KLnr),8(NC_Involved,Vnce#)
 1, 7.83d-3, 0, 0, 0, 0, 0, 0, 0, 0,  12, -1, 9, 1, 0, 0, 0, 0,  0, 0, 0, 0, 0, 0, 0, 0         !Fe>Fe(2+)+2e(-)
 2, 1.34d-17, 0, 0, 0, 0, 0, 0, 0, 0,   7, -1, 4, -1, 5, 1, 0, 0, 0, 0, 0, 0, 0, 0, 0, 0       !O2+4H(+)+4e(-)>4OH(-)
 3, 5.24d-7, 0, 0, 0, 0, 0, 0, 0, 0,   9, -1, 5, -2, 14, 1, 0, 0, 0, 0, 0, 0, 0, 0, 0, 0       !Fe(2+)+2OH(-)>Fe(OH)2
 4, 8.68d-8, 0, 0, 0, 0, 0, 0, 0, 0,   14, -4, 7, -1, 1, -2, 15, 4, 0, 0, 0, 0, 0, 0, 0, 0     !4Fe(OH)2+O2+2H2O>4Fe(OH)3
 5, 8.64d-2, 0, 0, 0, 0, 0, 0, 0, 0,   9, -4, 4, -4, 7, -1, 10, 4, 1, 2, 0, 0, 0, 0, 0, 0      !4Fe(2+)+4H(+)+O2>4Fe(3+)+2H20
 6, 1.59d-7, 0, 0, 0, 0, 0, 0, 0, 0,   10, -1, 5, -3, 15, 1, 0, 0, 0, 0, 0, 0, 0, 0, 0, 0      !Fe(3+)+3OH(-)>Fe(OH)3
 7, 3.57d-9, 0, 0, 0, 0, 0, 0, 0, 0,   10, -1, 6, -2, 18, 1, 0, 0, 0, 0, 0, 0, 0, 0, 0, 0      !Fe(3+)+2Cl(-)>FeCl2(2+)
 8, 2.13d-10, 0, 0, 0, 0, 0, 0, 0, 0,   18, -1, 1, -2, 14, 1, 4, 1, 6, 1, 0, 0, 0, 0, 0, 0     !FeCl2+2H20>Fe(OH)2+H(+)+Cl(-)
 9, 1.02d-10, 0, 0, 0, 0, 0, 0, 0, 0,   12, -1, 1, -1, 3, -1, 16, 1, 4, 1, 0, 0, 0, 0, 0, 0    !Fe+H2O+Cl(-)>FeCl(OH)(-)+H(+)+e(-)
10, 1.37d-13, 0, 0, 0, 0, 0, 0, 0, 0,  16, -1, 4, -1, 9, 1, 6, 1,  1, 1, 0, 0, 0, 0, 0, 0     !FeCl(OH)+H(+)>Fe(2+)+Cl(-)+H20
11, 5.8d-9, 0, 0, 0, 0, 0, 0, 0, 0,    19, 1, 2,-1, 3, -1, 0, 0, 0, 0, 0, 0, 0, 0, 0, 0         !Ca(2+)+CO3(2-)>CaCO3
12, 2.6d-14, 0, 0, 0, 0, 0, 0, 0, 0,   1, -1, 4, 1, 5, -1, 0, 0, 0, 0, 0, 0, 0, 0, 0, 0        !H2O>H(+)+OH(-)
13, 2.16d2, 0, 0, 0, 0, 0, 0, 0, 0,   4, -1, 5, -1, 1, 1, 0, 0, 0, 0, 0, 0, 0, 0, 0, 0        !H(+)+OH(-)>H2O
14, 1.09d-3, 0, 0, 0, 0, 0, 0, 0, 0,   8, -1, 6, -1, 20, 1, 0, 0, 0, 0, 0, 0, 0, 0, 0, 0      !Mg(2+)+Cl(-)>MgCl(-)
15, 5.5d-4, 0, 0, 0, 0, 0, 0, 0, 0,   20, -1, 8, 1, 6, 1, 0, 0, 0, 0, 0, 0, 0, 0, 0, 0        !MgCl(-)>Mg(2+)+Cl(-)
```

Input profile of our system at 323K varying potential from 0 to2V in 20 Steps

```
**********1D Problem******************
1              !=1 if planar; =2 if cylindrical; =3 if spherical
323            !Temperature(K)
**********Domain and Grid******************
0, 1.5, 250, 1.02      !XStt,XEnd(nm),Total # of divisions,Mesh-grading power
**********Involved Chemical Components*********
17     !Total#Of Involved Chemical Components
1, 2,3, 4, 5, 6, 7, 8, 9,10,12,14,15,16,18,19,20       !Above#X(ID_Glb Of Involved Chemical Component)
**********Involved Chemical Reactions*********
11     !Total#Of Involved Chemical Reactions
1,2,3,4,5,6,7,8,9,11,12,13,14,15       !Above#X(ID_Glb Of Involved Chemical Reaction)
**************Simulation Time & Steps**********************
20, 20         !NtotTimeSteps,NtotSnapShots
0              !ITimeStt(=0, first time run; >0, to restart based on ITimeStt-1 step)
*************Initial Uniform Concentrations**********************
32.76, 2.6d-3, 2.01d-3, 0.602d-7, 0.602d-7, 1.7d-4, 0, 0, 0,0,0,0,0,0,0, 0,0,0 !C(particle/nm^3)///MUST Follow the above order of involved chemical components
```

```
*************Boundary Condition*************
!---repeat below !NthC,Ramp1Jump2,2(Flux0_End,SpringCoef_End,C_Eqilibrium_End)
0, 1, 0, 1.d3, 2, 0, 1.d3, 0                    !electric (Displacement=Displacement0+Coef*(V-V0)) with displacement_unit:e/nm^2
1, 2, 0, 0, 0, 0, 1.d3, 32.76                   !chemical (flux=flux0+Coef*(C-C0)) with flux_unit:particle/nm^2/ns, and C_unit:particle/nm^3
2, 2, 0, 0, 0, 0, 1.d3, 2.6d-3                  !chemical (flux=flux0+Coef*(C-C0)) with flux_unit:particle/nm^2/ns, and C_unit:particle/nm^3
3, 2, 0, 0, 0, 0, 1.d3, 2.01d-3                 !chemical (flux=flux0+Coef*(C-C0)) with flux_unit:particle/nm^2/ns, and C_unit:particle/nm^3
4, 2, 0, 0, 0, 0, 1.d3, 0.602d-7                !chemical (flux=flux0+Coef*(C-C0)) with flux_unit:particle/nm^2/ns, and C_unit:particle/nm^3
5, 2, 0, 0, 0, 0, 1.d3, 0.602d-7                !chemical (flux=flux0+Coef*(C-C0)) with flux_unit:particle/nm^2/ns, and C_unit:particle/nm^3
6, 2, 0, 0, 0, 0, 1.d3, 1.2d-3
7, 2, 0, 0, 0, 0, 1.d3, 0                       !chemical (flux=flux0+Coef*(C-C0)) with flux_unit:particle/nm^2/ns, and C_unit:particle/nm^3
8, 2, 0, 0, 0, 0, 1.d3, 0                       !chemical (flux=flux0+Coef*(C-C0)) with flux_unit:particle/nm^2/ns, and C_unit:particle/nm^3
9, 2, 0, 0, 0, 0, 1.d3, 0                       !chemical (flux=flux0+Coef*(C-C0)) with flux_unit:particle/nm^2/ns, and C_unit:particle/nm^3
10, 2, 0, 0, 0, 0, 1.d3, 0                   !chemical (flux=flux0+Coef*(C-C0)) with flux_unit:particle/nm^2/ns, and C_unit:particle/nm^3
11, 2, 0, 0, 0, 0, 1.d3, 0                   !chemical (flux=flux0+Coef*(C-C0)) with flux_unit:particle/nm^2/ns, and C_unit:particle/nm^3
12, 2, 0, 0, 0, 0, 1.d3, 0                   !chemical (flux=flux0+Coef*(C-C0)) with flux_unit:particle/nm^2/ns, and C_unit:particle/nm^3
13, 2, 0, 0, 0, 0, 1.d3, 0                   !chemical (flux=flux0+Coef*(C-C0)) with flux_unit:particle/nm^2/ns, and C_unit:particle/nm^3
14, 2, 0, 0, 0, 0, 1.d3, 0                   !chemical (flux=flux0+Coef*(C-C0)) with flux_unit:particle/nm^2/ns, and C_unit:particle/nm^3
15, 2, 0, 0, 0, 0, 1.d3, 0
16, 2, 0, 0, 0, 0, 1.d3, 0
17, 2, 0, 0, 0, 0, 1.d3, 0
*************Numerical Parameters**********************
90000, 1.d-3, 1000, 0.0007      !IteratMax,ErrAllow,IteratDisplay,ARelax
**********************************************************************
************All Chemical Components**********************
20      !Total # of chemical components
--repeat (above #) below--!ID;Valance;Relative_Permittivity@Linear;StokesRadius;PhysicalRadius;EtaOverEpsil0((V/nm)^2-nS);AvdW0
 1,  0,   79, 0.09687,   0.1552,  0.113d1, 0.20294                      !H2O(0)(10)
 2,  2,    3,  0.0344,    0.099,  0.113d1, 0.20294                      !Ca(2+)(40)
 3, -2,    2, 0.03086,    0.178,  0.113d1, 0.20294                      !CO3(2-)(17)
 4,  1,    0,  0.0244,   0.1552,  0.113d1, 0.20294                      !H(1+)(1):CInf_H+=0.602d-7(pH=7)
 5, -1, 64.4,  0.0431,   0.137,  0.113d1, 0.20294                      !OH(1-)(9):CInf_OH-=0.602d-7(pH=7)
 6,  -1,   10, 0.1082,    0.181,  0.113d1, 0.20294                      !Cl(1-)(17)
 7, 0, 6.89,   0.109,   0.135 , 0.113d1, 0.20294                       !O2(16)
 8,  2,  7.6,   0.311,    0.072, 0.113d1, 0.20294                       !Mg(2+)
9,  2,   16,  0.3851,    0.06,  0.113d1, 0.20294                       !Fe(2+)(26)
10,  3, 15.8,  0.3861,   0.07,   0.113d1, 0.20294                      !Fe(3+)
 11,  0, 15.1,   0.213,    0.161, 0.113d1, 0.20294                      !HCl
 12,  1,   16,  0.3851,    0.126,  0.113d1, 0.20294                     !Fe
 13,  1, 14.2,   0.164,    0.216, 0.113d1, 0.20294                      !FeOH(+1)
 14,  0, 14.2,   0.165,   0.369,  0.113d1, 0.20294                      !Fe(OH)2
 15, 0, 14.2,   0.380,   0.382,  0.113d1, 0.20294                       !Fe(OH)3
16,  1, 13.8,  0.4613,   0.2246, 0.113d1, 0.20294                      !Fe(OH)Cl(1+)
 17,  2, 14.6,  0.4613,   0.2246, 0.113d1, 0.20294                     !FeCl(2+)
18,  1, 14.6,  0.4613,   0.2246, 0.113d1, 0.20294                      !FeCl2
19, 0,  9.1,   0.0344,   0.0348,  0.113d1, 0.20294                     !CaCO3
20,  1,  5.6,   0.311,   0.1847, 0.113d1, 0.20294                      !MgCl(1+)
------------------------------------------------------------------------
************All Chemical Reactions**********************
15      !Total # of Chemical Reactions
--repeat (above #) below--ID,KConst(MUST be consistent to generate rate by particle/nm^3/ns),4(NCLnr,KLnr),8(NC_Involved,Vnce#)
 1, 7.83d-3, 0, 0, 0, 0, 0, 0, 0, 0,  12, -1, 9, 1, 0, 0, 0, 0,  0, 0, 0, 0, 0, 0, 0, 0         !Fe>Fe(2+)+2e(-)
 2, 1.34d-17, 0, 0, 0, 0, 0, 0, 0, 0,   7, -1, 4, -1, 5, 1, 0, 0, 0, 0, 0, 0, 0, 0, 0, 0       !O2+4H(+)+4e(-)>4OH(-)
 3, 5.24d-7, 0, 0, 0, 0, 0, 0, 0, 0,   9, -1, 5, -2, 14, 1, 0, 0, 0, 0, 0, 0, 0, 0, 0, 0       !Fe(2+)+2OH(-)>Fe(OH)2
 4, 8.68d-8, 0, 0, 0, 0, 0, 0, 0, 0,   14, -4, 7, -1, 1, -2, 15, 4, 0, 0, 0, 0, 0, 0, 0, 0     !4Fe(OH)2+O2+2H2O>4Fe(OH)3
 5, 8.64d-2, 0, 0, 0, 0, 0, 0, 0, 0,   9, -4, 4, -4, 7, -1, 10, 4, 1, 2, 0, 0, 0, 0, 0, 0      !4Fe(2+)+4H(+)+O2>4Fe(3+)+2H20
 6, 1.59d-7, 0, 0, 0, 0, 0, 0, 0, 0,   10, -1, 5, -3, 15, 1, 0, 0, 0, 0, 0, 0, 0, 0, 0, 0      !Fe(3+)+3OH(-)>Fe(OH)3
 7, 3.57d-9, 0, 0, 0, 0, 0, 0, 0, 0,   10, -1, 6, -2, 18, 1, 0, 0, 0, 0, 0, 0, 0, 0, 0, 0      !Fe(3+)+2Cl(-)>FeCl2(2+)
 8, 2.13d-10, 0, 0, 0, 0, 0, 0, 0, 0,   18, -1, 1, -2, 14, 1, 4, 1, 6, 1, 0, 0, 0, 0, 0, 0     !FeCl2+2H20>Fe(OH)2+H(+)+Cl(-)
 9, 1.02d-10, 0, 0, 0, 0, 0, 0, 0, 0,   12, -1, 1, -1, 3, -1, 16, 1, 4, 1, 0, 0, 0, 0, 0, 0    !Fe+H2O+Cl(-)>FeCl(OH)(-)+H(+)+e(-)
10, 1.37d-13, 0, 0, 0, 0, 0, 0, 0, 0,  16, -1, 4, -1, 9, 1, 6, 1,  1, 1, 0, 0, 0, 0, 0, 0      !FeCl(OH)+H(+)>Fe(2+)+Cl(-)+H20
11, 5.8d-9, 0, 0, 0, 0, 0, 0, 0, 0,    19, 1, 2,-1, 3, -1, 0, 0, 0, 0, 0, 0, 0, 0, 0, 0         !Ca(2+)+CO3(2-)>CaCO3
12, 2.6d-14, 0, 0, 0, 0, 0, 0, 0, 0,   1, -1, 4, 1, 5, -1, 0, 0, 0, 0, 0, 0, 0, 0, 0, 0        !H2O>H(+)+OH(-)
13, 2.16d2, 0, 0, 0, 0, 0, 0, 0, 0,   4, -1, 5, -1, 1, 1, 0, 0, 0, 0, 0, 0, 0, 0, 0, 0         !H(+)+OH(-)>H2O
14, 1.09d-3, 0, 0, 0, 0, 0, 0, 0, 0,   8, -1, 6, -1, 20, 1, 0, 0, 0, 0, 0, 0, 0, 0, 0, 0      !Mg(2+)+Cl(-)>MgCl(-)
15, 5.5d-4, 0, 0, 0, 0, 0, 0, 0, 0,   20, -1, 8, 1, 6, 1, 0, 0, 0, 0, 0, 0, 0, 0, 0, 0        !MgCl(-)>Mg(2+)+Cl(-)
```

References

1. Modelling Pitting Corrosion in Carbon Steel by Suhella Salleh, School of Materials, University of Manchester
2. Ahmad, Z., Principles of Corrosion Engineering and Corrosion Control. 2006: Butterworth-Heinemann.
3. Ergun, M., Akcay, L., Investigation of pitting potential of carbon steel using experimental design method. British Corrosion Journal, 2002. **37**(3): p. 235-238.
4. Corrosion of Steel, Aluminum and Copper in Electrical Applications By: Alex Mak, P. Eng. - Senior Field Applications Engineer, General Cable
5. Fluoridation of Drinking Water and Corrosion of Pipes in Distribution Systems Fact Sheet
   http://www.cdc.gov/fluoridation/factsheets/engineering/corrosion.htm
6. Study Made Social- Flint Study
   http://flintstudy.com/
7. The Electrical Double Layer and Its Structure by Zbigniew Stojek(2009)
8. Electrical Double Layer
   http://web.nmsu.edu/~snsm/classes/chem435/Lab14/double_layer.html
9. Library kinetics of Aqueous Corrosion
   http://www.doitpoms.ac.uk/tlplib/aqueous_corrosion/double_layer.php
10. Electric Double Layer

http://faculty.kfupm.edu.sa/ME/hussaini/Corrosion%20Engineering/02.05.04.htm

11. Stress, Flow and Diffusion in an Electrical Double Layer of Ion-dipole Mixtures by B. Yang, Department and Mechanical and Aerospace Engineering, University of Texas at Arlington, Arlington, Texas, USA
12. Carnahan, N. F. & Starling, K. E. Equation of state for nonattracting rigid spheres. *The Journal of chemical physics* **51**, 635-636 (1969).
13. Melcher, J. R. *Continuum electromechanics*. Vol. 2 (MIT press Cambridge, 1981)
14. Three strategies for combating the corrosion of steel pipes carrying desalinated potable water by A.M. Shams El Din, Laboratory of Electrochemistry and Corrosion, National Research Centre, Dokki, Cairo, Egypt.
15. Water Encyclopedia http://www.waterencyclopedia.com/En-Ge/Fresh-Water-Natural-Composition-of.html
16. Metal flux and dynamic speciation at (bio)interfaces. Part I: Critical evaluation and compilation of physico-chemical parameters for complexes with simple ligands and fulvic/humic substances by Jacques Buffle*, Zeshi Zhang, Konstantin Startchev Analytical and Biophysical Environmental

Chemistry (CABE), University of Geneva, Sciences II, 30 quai E. Ansermet, CH-1211 Geneva 4

17. On the molecular diffusion coefficients of dissolved CO2; HCO 3 , and CO2 3 and their dependence on isotopic mass Richard E. Zeebe , School of Ocean and Earth Science and Technology, University of Hawaii at Manoa, 1000 Pope Road, MSB 504, Honolulu, HI 96822, USA
18. Dielectric Constants of various materials. http://www.clippercontrols.com/pages/Dielectric-Constant-Values.html
19. Basic Mechanisms of Corrosion and Corrosion Control for Water and Wastewater Systems Graham E.C. Bell, Ph.D., P.E.

Biographical Information

The author completed his Bachelor in engineering degree in mechanical engineering at University of Mumbai. While there, he conducted research in Aerodynamics and modeling of flying wings. He attended the University of Texas at Arlington for his Master of Science degree in mechanical engineering. During his studies at UTA, she conducted research under the guidance of Dr. Yang on Corrosion and Electric Double Layer Structures. The author is strongly interested in finite element analysis and structural mechanics.